19

Desing of Multiphase Boost Converter for Hybrid Fuel Cell/Battery Power Sources

Dr Miroslav Lazić[1], Dr Miloš Živanov[2] and Boris Šašić[3]
[1]*Iritel.AD Beograd,*
[2]*FTN Novi Sad,*
[3]*Spellman New York*
[1,2]*Serbia*
[3]*USA*

1. Introduction

Alternative energy sources are becoming less and less "alternative". Recent decade has been underlined with worldwide efforts in finding suitable long term alternatives to the carbon based energy sources. There is a multitude of very compelling reasons for investing extra effort – limited supply of natural resources, environmental, geopolitical and even economical reasons.

Sun, wind and oceans are all being harnessed to provide stable and reliable energy. That energy is converted for immediate use or for storage in supercapacitors, chemical energy sources or as a derived chemicals (Hydrogen is produced, for instance).

Next link in the alternative energy chain is efficient use. New supercapacitors are being developed and there are many different battery types already available on the market, each with its own unique application that optimizes efficiency of chemical conversion and number of charge/discharge cycles with minimum of capacity loss.

Fuel cells are being used to efficiently reclaim energy stored in Hydrogen. The process has been well known for decades and is being used in power generation industry in high power systems. As the technology advanced, lower power applications were found – chemical industry was a big benefactor: most of the exhaust gasses could be reclaimed and have Hydrogen extracted in a simple, cost effective manner, ensuring a free energy supply once initial investment in fuel cells and regenerators has been made.

Development of new materials helped further reduce costs and increase efficiency, and even low power fuel cells are now widely available. Even though there are still many new and exciting ongoing developments, the technology is now considered mature and ready for prime time. Fuel cells have a good history in many applications (chemical industry, power generation, transportation) and is considered a serious contender in many other industries.

In some of these industries fuel cells will gain faster acceptance than in others. Material handling industry is among those where benefits of fuel cells can be easily documented and increased cost of initial implementation justified. A fuel cell based system that replaces standard forklift battery pack has many advantages, such as: fast refueling, longer run time between refueling, longer life of the energy source and low maintenance requirements.

In a typical electric vehicle fuel cells are augmented by an energy storage element, such as a supercapacitor, flywheel or battery. Such hybrid system makes some of the fuel cell deficiencies (high output impedance, for example) transparent to the final user. The typical systems used in industrial vehicles use battery as the energy storage component.
A critical part of such fuel cell system is the load regulator. Its main role is to enable controlled current draw from the fuel cell. It also needs to maintain the auxiliary batteries in a fully charged state and to regulate load current.
This thesis illustrates work on overcoming major challenges of fuel cell load regulator design and offers an illustration in the form of a practical realization of a 5kW unit with application in industrial electric vehicles.

2. Fuel cell systems

A fuel cell is an electrochemical power source that converts chemical fuel into electrical energy. The electricity is generated via reactions between the fuel and an oxidant (so called reactants) in the presence of an electrolyte. The reactants flow into the cell, and the reaction products flow out of it, while the electrolyte remains within it. The electrolyte is a substance specifically designed so ions can pass through it, but the electrons cannot.
Unlike conventional electrochemical batteries, fuel cells consume reactant from an external source, and it must be replenished, as long as the reactant is available the power can be generated, there are no other restrictions on the fuel cell "capacity". By contrast, batteries store electrical energy chemically and have limited capacity.Hydrogen based fuel cells are the most common. They use Hydrogen as the fuel and Oxygen as the oxidant. Oxygen is most commonly used from air. Many other combinations of fuels and oxidants are possible, but they are not widely utilized.

2.1 Principle of fuel cell operation

The core of a fuel cell consists of a membrane electrode assembly, which is placed between two flow-field plates. The assembly consists of two electrodes, the anode and cathode, separated by a Proton Exchange Membrane (PEM). The block diagram of a fuel cell is shown in Figure 1.

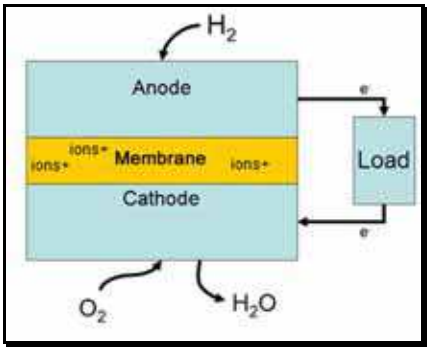

Fig. 1. Fuel cell block diagram

The two electrodes are coated with thin layer of Platinum that acts as a catalyst. At the anode, the catalyst oxidizes the fuel (Hydrogen), turning it into a positively charged ion and a negatively charged electron. The membrane (PEM) is designed so that ions can pass

through it, but the electrons cannot. The freed electrons travel through a wire creating the electrical current. The ions travel through the electrolyte to the cathode. Once reaching the cathode, the ions are reunited with the electrons and the two react with a third chemical, usually oxygen, to create water and heat.
A typical fuel cell produces a voltage of 0.6 - 0.7V at full rated load. Voltage decreases as current increases, due to several factors:

- Activation loss (activation polarization)
- Ohmic Polarization (voltage drop due to resistance of the cell components and interconnects)
- Gas transport loss (depletion of reactants at catalyst sites under high loads, causing rapid loss of voltage).

A typical fuel cell load curve is shown in Figure 2.

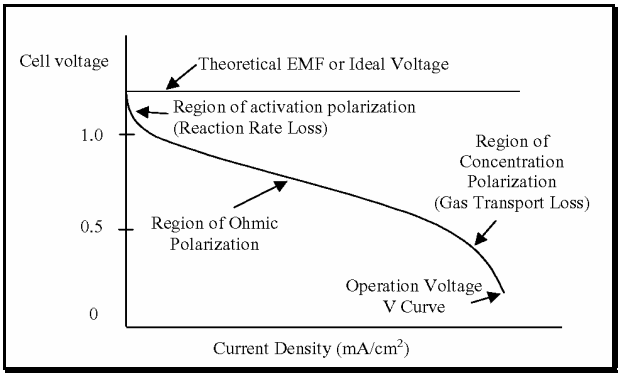

Fig. 2. A typical fuel cell load curve

To deliver the desired amount of energy, the fuel cells can be combined in series and parallel circuits. Such a design is called a fuel cell stack.
A few different fuel stacks are shown in Figure 3.

Fig. 3. Examples of fuel cell stacks

2.2 Fuel cell systems

As discussed in the Introduction, the thesis will concentrate on fuel cell applications for industrial off road vehicles. Electric forklifts (Figure 4) are especially interesting due to the problems with existing battery packs.

Fig. 4. Electric forklift

A fuel cell based system that replaces standard forklift battery pack has many advantages, such as: fast refueling, longer run time between refueling, longer life of the energy source and low maintenance requirements.

In a typical electric vehicle fuel cells are augmented by an energy storage element, such as supercapacitor, flywheel or battery. Such hybrid system makes some of the fuel cell deficiencies (the most important one being high output impedance) transparent to the final user.

Hybrid systems with a small lead acid battery have many advantages in material handling applications. The most significant two are: (1) battery provides peak current handling capabilities and (2) it ensures reserve power to drive the vehicle to refueling station should hydrogen tank be completely depleted.

Block diagram of a hybrid fuel cell system using auxiliary Sealed Lead-Acid (SLA) battery is shown in Figure 5.

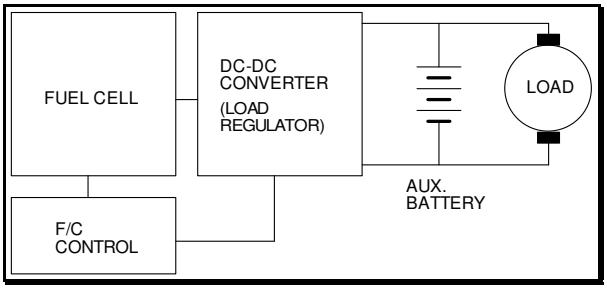

Fig. 5. Block diagram of a hybrid fuel cell system

Fuel cell is used as a main energy source, controlled by a dedicated electronics (**F/C Control**) that controls main aspects of fuel cell operation – Hydrogen flow and pressure, monitors output voltage and current and sets operating parameters of a fuel cell regulator. The **load regulator** processes raw power from the fuel cell, converting it into levels suitable for the load, while keeping auxiliary battery charged and providing adequate protections of the fuel cell, load and self-protection against overvoltage, overtemperature and overload. **Auxiliary battery** is a small (70Ah) Sealed lead-Acid battery with the main purpose to provide peak power when demanded by the load. Typical peak loads are during vehicle's rapid acceleration and lifting heavy loads. If the Hydrogen tank goes empty, the battery also provides backup power sufficient to drive the vehicle to the refueling station. Finally, the system's **load** comprises forklift's traction motor, hydraulic pumps, lift motors and various communication and control electronics: new generations of forklifts bear very little resemblance to the noisy and slow vehicles of the past – typical rider vehicle (Class I or Class II) in a larger fleet has a sophisticated joystick controls, very informative displays, radio communication equipment, GPS and tracking devices, and the total power draw is not negligible.

2.3 Specification requirements

There are two main factors influencing every design: electrical specifications and application based details. Electrical specifications are straightforward and require little explanation. For our particular design, a fuel cell regulator, electrical specifications are fairly simple:

- Maximum power: 5,5kW
- Input voltage range: 24-36V
- Output voltage range: 36-60V
- Maximum output current: 150A

Specification parameters related to this particular application add more clarity regarding expected performance of the final product. The parameters are not always clearly defined by numbers and physical values – most common examples are "small size", "low cost", etc. Regardless of their ambiguity or lack of definition, they are still valuable information that is specific to the application and affects the design process.

In this case application specific requirements are summarized as:

- Continuously variable control with automatic crossover:
- Input current controlled in the range 0-220A
- Low input current ripple: <1% of output current, measured with 0-10kHz bandwidth (critical for longevity of the fuel cell)
- High efficiency: 94% min at 2kW and 96% above 2.5kW
- Protection against reverse current (which may cause temperature rise and hazardous pressure build up)
- Ability to sustain peak load currents of up to 800A for short period of time (1-5 seconds)
- Operating ambient temperature -30 to +60°C
- Low physical profile (load regulator needs to fit into a predefined space)
- Low cost

3. Multiphase boost converters

Boost converter belongs to the family of basic power conversion topologies (the other two being buck and buck-boos derivative). Boost converters are probably the most versatile

power converters today. They cover power range from fraction of a Watt (for example raising a single cell battery voltage to a 3.3 or 5V logic levels in portable equipment) to tens of kW (alternative energy sources and distributed power). Extremely popular and almost exclusively used in Power Factor Correction (PFC) applications, they are being manufactured in millions of units.

Unlike buck converter, boost topology is somewhat more difficult to control, due to the Right Half Plane (RHP) Zero in the control transfer function. RHP Zero sets practical limits on the control loop bandwidth but.

Another comparative disadvantage is no inherent short circuit protection: if the output terminals are shorted there is nothing (other than circuit parasitic) to limit or interrupt short circuit current.

Over time, designers have learned how to deal with the two major drawbacks mentioned above and today there are very few restrictions for practical use of this topology.

The boost converter is well understood and successfully used in the multitude of applications. It is typically used when output voltage needs to be higher than the input voltage.

Introduction of multiphase topologies has expanded field of practicality for the converters by offering many advantages that will be discussed below. The simplest way of describing a multistage converter is to see it as consisting of several power stages (converter "phases") with inputs and outputs connected in parallel and drive signals shifted to ensure uniform distribution over a switching period – this techniques is also known as "interleaving" and the term will be used throughout this work.

Input inductance of the boost converter helps control current ripple and has positive effects on reducing electromagnetic emissions. However, the size of the inductor is proportional to the inductance and the square of the peak current and for high power applications its size is considerable.

For high power converters operating from relatively low input voltages, inductor current can be limiting factor due to the fairly large size and lack of space or even availability of adequate core sizes.

One way to reduce the inductor's size would be running the converter at high frequency. Unfortunately, for high power converters, practical considerations such as core's eddy current losses, switching losses in the power switch and rectifier and electromagnetic emissions severely limit the maximum switching frequency.

Output capacitor in the boost converter is subjected to large variations of the current through them. Capacitors' peak-to-peak current is equal to the sum of the input inductor peak current and load current. Consequently, the RMS value of the capacitor current is high resulting in high stress, heating and reduced life and overall reliability of the unit.

One way to deal with the problems is by designing multiphase, interleaved power stages. In a typical interleaved converter several power stages are connected in parallel and driven with signals shifted by 360°/(number of phases). Effective switching frequency is, thus, increased proportionally to the number of phases with several important benefits:

- For the same value of inductance (compared to an equivalent single-phase boost), current ripple is significantly reduced, helping reduce size of the inductor;
- For the same ripple current, individual inductors can have lower inductance, again reducing their size;
- Reduced ripple current helps relieve stress on the output filter capacitors and increased effective switching frequency makes capacitors running closer to their optimum (most of the aluminum electrolytic capacitors have increased RMS current rating as frequency increases).

3.1 Single-phase boost converter

This is the standard boost converter. Simplified schematic of the power train is shown in Figure 6.

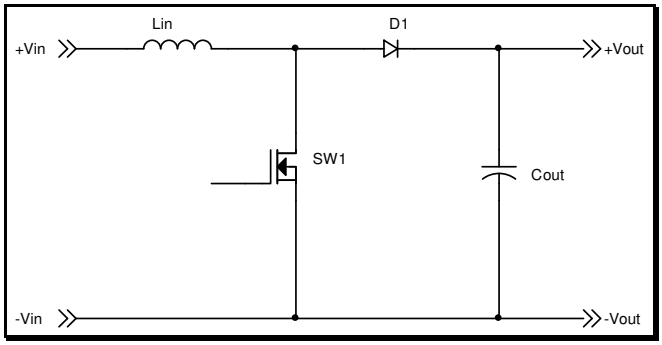

Fig. 6. Boost converter schematic

This is the basic and most commonly used variation, typical for low power converters as well as medium to high power PFC designs. The reason for its popularity is obvious – simplicity with low parts count makes this an inexpensive and reliable solution. Additionally, the topology has typically high conversion efficiency thanks to its simplicity and principle of operation: in normal operation, at any moment within a switching cycle current flows through only one semiconductor part (it alternates between the switch and the rectifier). This is can be seen in Figure 7 that shows main waveforms.

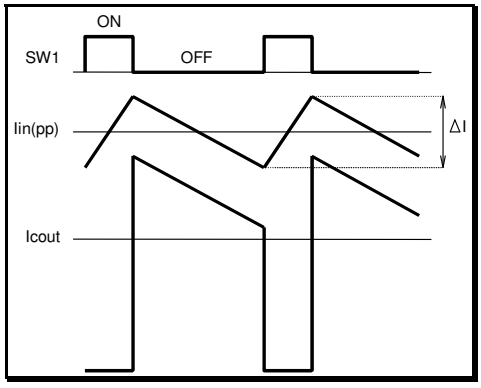

Fig. 7. Boost converter input current and output capacitor waveforms

Basics of the boost converter operation are well known and easily accessible so they will be omitted from this work.

Specific requirements of the application which can be described in simplest terms as "low voltage- high current", dictate that special attention is paid to the current loading of components. As seen in Figure 6, there are only four components employed by the basic topology, two semiconductor switches, inductor and capacitor. Naturally, there will be a lot more parts in the final design, but properly defining critical parameters for the four components will make a selection process for the rest pretty straightforward.

Semiconductor switches, shown in the schematics (Figure 6) as MOSFET and a diode are less critical of the four indicated components. Modern semiconductor have high current density in miniature packaging and major constraint is not their current handling capacity – rather it is power dissipation that small package can conduct to the ambient. Starting with power loss budget, derived from desired efficiency, it will be fairly easy to make proper selection of the component type and quantity.
Unlike semiconductors, where achieving adequate design margins is not a difficult process, inductors and capacitors present a bigger challenge. Even though material science has brought new materials, inductors and capacitors have seen slower progress.
Relationship between power dissipation and saturation characteristics is still a limiting factor for an inductor design, directly affecting its size and operating temperature. Electrolytic capacitors are still the best part for controlling output voltage ripple, but their life is severely limited by temperature rise due to high ripple currents.In order to make proper selection of adequate parts, the work will concentrate on defining input inductor and output capacitor current ripple and defining a method for their optimization.

3.1.1 Input current ripple

For a single phase boost converter input current (I_{in}) is same as the input inductor current (I_{Lin}). All input variables and component designations in the following equations are referenced to Figure 6, and δ is operating duty cycle of the active switch, defined as turn-on time (T_{on}) divided by switching period (T).
Rising slope of the inductor current is given as

$$k_{Lin} = \frac{V_{in}}{L_{in}} \tag{1}$$

Inductor peak-to-peak current ripple is

$$\Delta I_{Lin} = k_{Lin}\delta T = \frac{V_{in}}{L_{in}}\delta T \tag{2}$$

where δ represents main switch duty cycle and $T=T_{on}+T_{off}$ is the switching period.

$$\delta = \frac{T_{on}}{T_{on} + T_{off}} \tag{3}$$

Substituting V_{in} from the equation for the boost converter's DC gain (Eq. (4) below) into Eq. (2)

$$\frac{V_{out}}{V_{in}} = \frac{1}{1-\delta} \tag{4}$$

the final equation for the inductor ripple current is derived as

$$\Delta I_{Lin} = \delta(1-\delta)\frac{V_{out}T}{L_{in}} \tag{5}$$

3.1.2Output capacitor RMS current

Most commonly used method for calculating RMS values of typical power converter waveforms is by splitting it into piecewise segments and then adding squared RMS values of each individual segment. That is the method that will be used for multiphase converters. The method certainly works for single phase converters as well, but there is a more elegant alternative: we can resort to a Kirchoff's Law's equivalent for RMS currents and calculate output capacitor current by considering all RMS currents inside a boost converter:

$$I_{CoRMS}^2 = I_{inRMS}^2 - I_{swRMS}^2 - I_{out}^2 \tag{6}$$

Where,

$$I_{inRMS} = I_{LinRMS} = I_{inAVG}\sqrt{1+\frac{1}{3}\left(\frac{\Delta I_{Lin}}{2I_{inAVG}}\right)^2} \tag{7}$$

$$I_{swRMS} = I_{inAVG}\sqrt{\delta\left(1+\frac{1}{3}\left(\frac{\Delta I_{Lin}}{2I_{inAVG}}\right)^2\right)} \tag{8}$$

then, finally,

$$I_{CoRMS}^2 = (1-\delta)I_{inAVG}^2\left(1+\frac{1}{3}\left(\frac{\Delta I_{Lin}}{2I_{inAVG}}\right)^2\right) - I_{out}^2 \tag{9}$$

The average input current for an ideal, lossless converter can be calculated by starting with a premise that input power equals the output power:

$$I_{inAVG} = \frac{V_{out}I_{out}}{V_{in}} = \frac{V_{out}I_{out}}{V_{out}(1-\delta)} = \frac{1}{(1-\delta)}I_{out} \tag{10}$$

Substituting equations (5) and (10) into (9), we are getting the closed form equation for the output capacitor RMS current as follows:

$$I_{CoRMS}^2 = \frac{\delta}{1-\delta}I_{out}^2 + \frac{1}{12}\delta^2(1-\delta)^3\left(\frac{V_{out}T}{L_{in}}\right)^2 \tag{11}$$

As δ is always less than one, the right hand side of the equation can be neglected with only a small negative effect on overall accuracy. Practical illustration of this simplification is that the AC ripple component is neglected, i.e. considered negligible when compared to the average value of the input inductor current, which is a meaningful and common practice in everyday engineering. This simplification will pay large dividends when multiple phases are analyzed, as the complete closed form equations would otherwise be difficult to manage and understand. Also the practical measurements will show that, in an optimized multiphase converter, the ripple is indeed very small when compared to the average input current. The identical simplification will be used for deriving RMS capacitor current equations for multiphase converters. It should be noted, though, that this simplification will

result in capacitor ripple current being zero at specific values for duty cycle. In reality, the ripple current will never reach zero but the actual value will be equal to the neglected factor in the above equation.
Simplified Eq. (11) is then:

$$I_{CoRMS}^2 = \frac{\delta}{1-\delta} I_{out}^2 \tag{12}$$

3.2 Two-phase interleaved boost converter

By adding another power stage, connecting inputs and outputs in parallel and shifting drive signals by 180° a two phase interleaved boost converter is created. Principle schematics is shown in Figure 8.

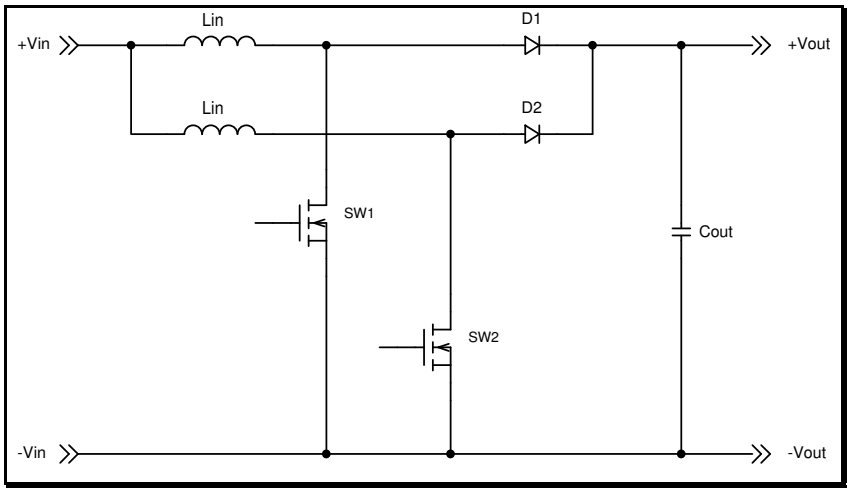

Fig. 8. Two phase boost converter

For a two-phase interleaved boost converter, two distinct modes of operation can be analyzed. One is for duty cycles lower than 0.5 (50%) and the other one for duty cycles above 0.5. At exactly 0.5 the converter benefits from ripple cancellation and input current ripple is zero, while output capacitor ripple is at minimum (although not exactly zero, as explained in 3.2). The two modes of operation are illustrated in Figures 9 and 10.

- **Input current ripple**
  The input current ripple, ΔI_{in} will be analyzed for the two cases, $\delta<0.5$ and $\delta>0.5$.
- **$\delta<0.5$**
  Input current and input inductor current waveforms for a duty cycle below 0.5 are shown in Figure 9. For the sake of clarity, designations for ripple currents and duty cycles are removed from the graphs, as they are similar to the single stage boost diagrams.
  The duration of the rising slope of the input current equals the rising time of an individual inductor's current, i.e. δT. The input current ripple's rising slope in this interval is a difference of the rising current slope of one inductor and falling slope of the other one:

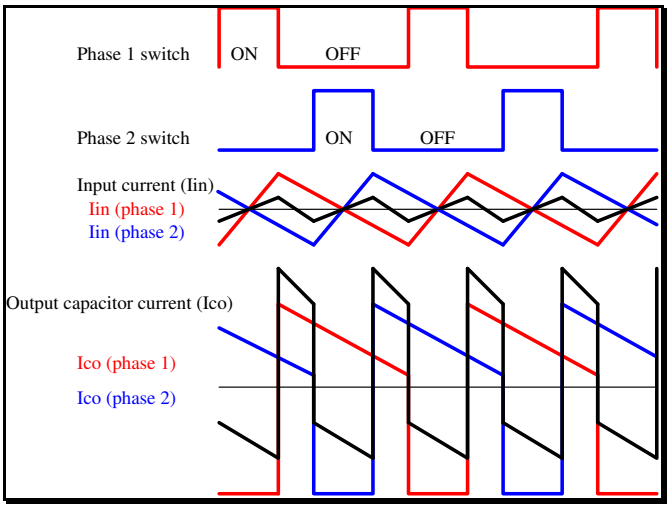

Fig. 9. Two phase boost converter w-forms for δ<0.5

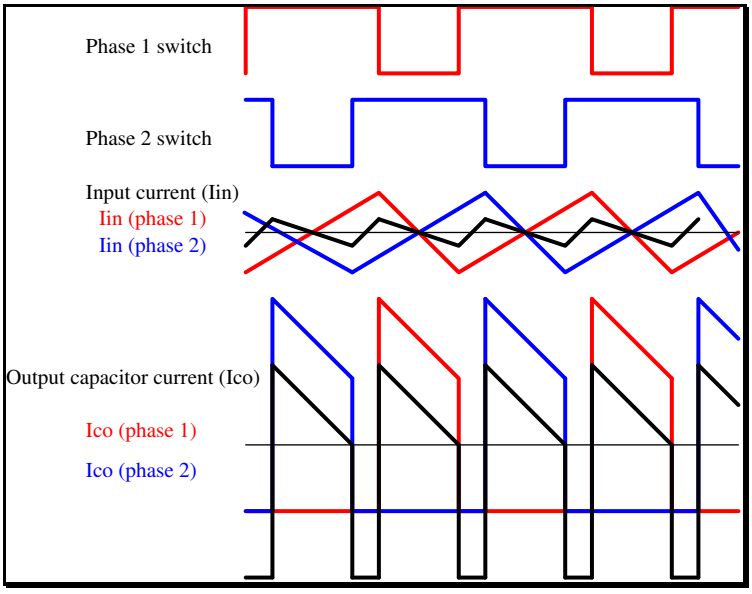

Fig. 10. Two phase boost converter w-forms for δ>0.5

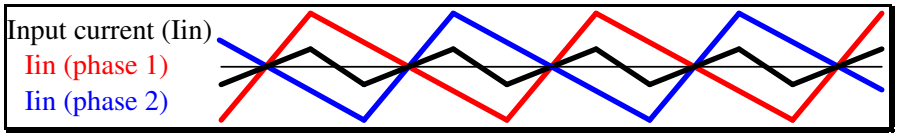

Fig. 11. Two-phase boost converter - input current waveforms, δ<0.5

$$k_{in} = k_{on} - k_{off} = \frac{V_{in}}{L_{in}} - \frac{(V_{out} - V_{in})}{L_{in}} \tag{13}$$

Peak-to-peak input current ripple is:

$$\Delta I_{in} = k_{in}\delta T \tag{14}$$

Substituting V_{in} from (4) the input current ripple for δ<0.5 is derived as:

$$\Delta I_{in} = \delta(1-2\delta)\frac{V_{out}T}{L_{in}} \tag{15}$$

- **δ>0.5**
  Input current waveforms for δ>0.5 are shown in Fig. 12.

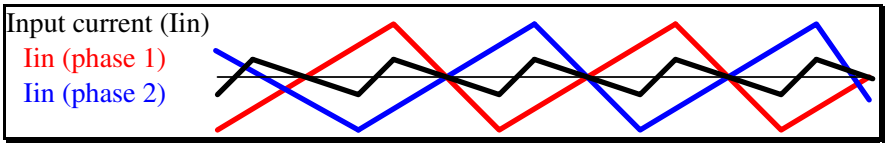

Fig. 12. Two-phase boost converter - input current waveforms, δ>0.5

The duration of the input current rising slope in this case equals T/2-(1-δ)T, or (δ-1/2)T. The slope equals:

$$k_{in} = 2k_{onoff} = 2\frac{V_{in}}{L_{in}} \tag{16}$$

And the input current is:

$$\Delta I_{in} = k_{in}(\delta - \frac{1}{2})T = \left(\delta - \frac{1}{2}\right)(2-2\delta)\frac{V_{out}T}{L_{in}} \tag{17}$$

- **Output capacitor RMS current**
  Similar process will be followed in analyzing current ripple in the output filter capacitor.
- **δ<0.5**
  Output capacitor current waveform for δ<0.5 is shown in Fig. 13.
  By neglecting the input inductor ripple, the waveform gets the rectangular shape. This approximation (discussed in 3.2) is acceptable as it helps get results which are easier to understand and interpret. Loss of accuracy is negligible when compared to tolerances and required design margins. Positive amplitude of the waveform equals (I_{inAVG}-I_{out}) and negative amplitude is (I_{out}-I_{inAVG}/2). The signal is negative during time that equals δT and positive during time (1/2-δ)T. RMS current is then calculated starting with:

$$I_{CoRMS}{}^2 = \delta\left(I_{out} - \frac{I_{inAVG}}{2}\right)^2 + \left(\frac{1}{2} - \delta\right)(I_{inAVG} - I_{out})^2 \tag{18}$$

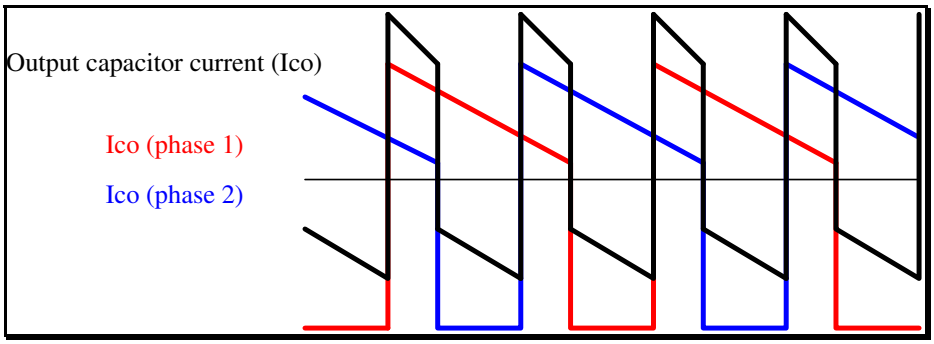

Fig. 13. Two-phase boost converter - output capacitor current waveforms, δ<0.5

Substituting Eq. (10), the final result is derived as

$$I_{CoRMS} = \frac{I_{out}}{2(1-\delta)}\sqrt{\delta(1-\delta)} \tag{19}$$

- **δ>0.52**

The output capacitor's current waveform is shown in Figure 14.

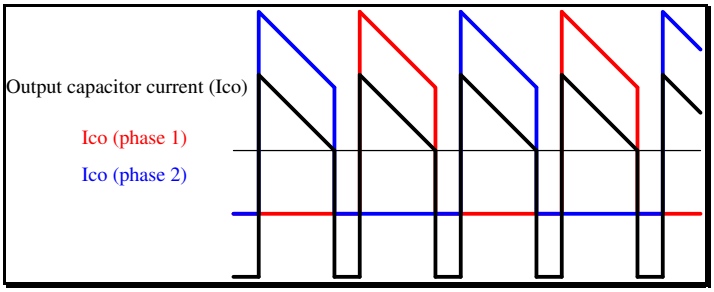

Fig. 14. Two-phase boost converter - output capacitor current waveforms, δ>50%

Positive amplitude of the simplified waveform is now ($I_{inAVG}/2 - I_{out}$), duration is (1-δ)T. Negative amplitude equals I_{out} and duration is (δ-1/2)T. RMS current is, therefore,

$$I_{CoRMS}^2 = \left(\delta - \frac{1}{2}\right) I_{out}^2 + (1-\delta)\left(\frac{I_{inAVG}}{2} - I_{out}\right)^2 \tag{20}$$

Final equation is derived as

$$I_{CoRMS} = \frac{I_{out}}{2(1-\delta)}\sqrt{\frac{1}{2}(2\delta-1)(2-2\delta)} \tag{21}$$

3.3 Three-phase interleaved boost converter

Current state of research and industry applications indicates that most commonly used number of phases in multiphase converters is two, three, or multiple of either one (4, 6, etc.).

or that reason and in order to make it easier to derive generalized equations for multiphase converters the three phase boost will also be addressed in more detail.
Basic schematic is shown in Figure 15 and it represents three interleaved stages with drive signals shifted by 120°.

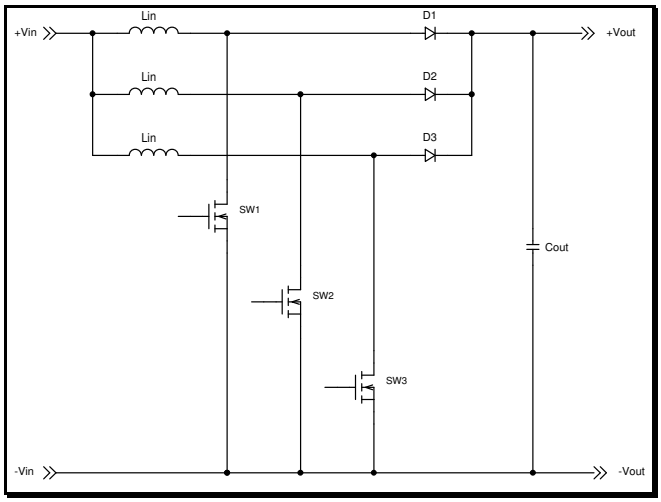

Fig. 15. Three phase boost converter

Similarly to the analysis of a two phase interleaved converter, for the three phase boost converter there are three modes of operation of interest: (1) $\delta<1/3$; (2) $1/3<\delta<2/3$ and (3) $\delta>2/3$. Input current waveforms of a three-phase boost converter with duty cycles within the described ranges are shown in Figures 16, 17 and 18.

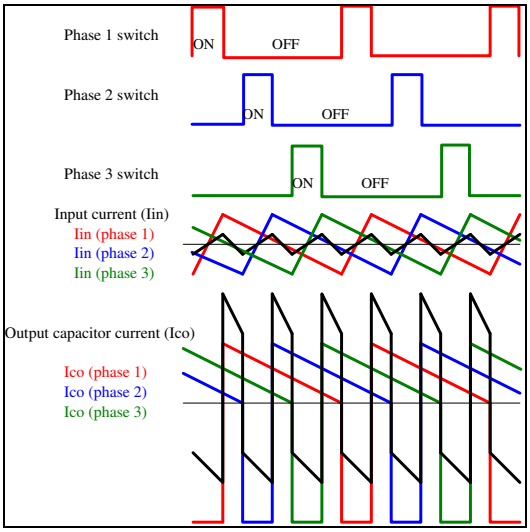

Fig. 16. Three-phase boost converter w-forms for $\delta<1/3$

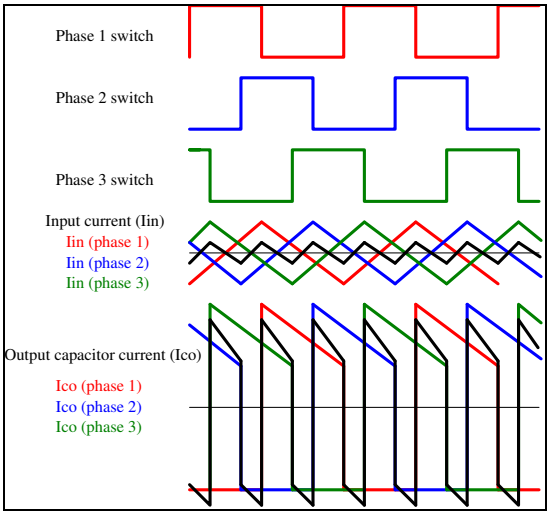

Fig. 17. Three phase boost w-forms for 1/3<δ<2/3

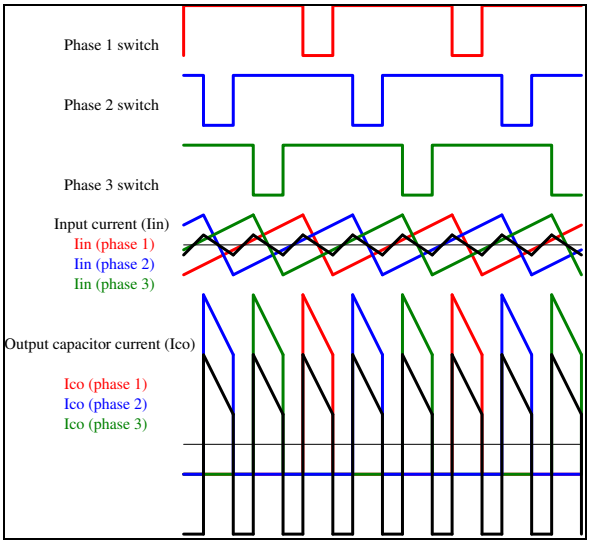

Fig. 18. Three phase boost w-forms for δ>2/3

3.3.1 Input current ripple

- **δ<1/3**

  Input current and input inductor current waveforms for a duty cycle below 1/3 are shown in Figure 19.

  In this case the duration of the input current's rising slope coincides with the ON time of the main switch, δT. The slope itself can be calculated in the similar manner as in the two phase configuration:

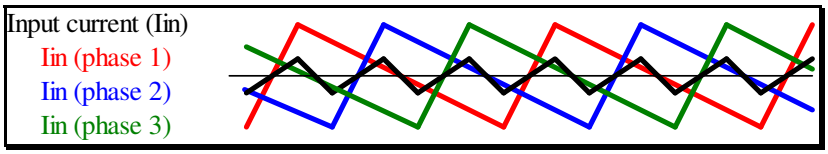

Fig. 19. Three-phase boost converter - input current waveforms, δ<1/3

$$k_{in} = k_{on} - 2k_{off} = \frac{V_{in}}{L_{in}} - 2\frac{(V_{out} - V_{in})}{L_{in}} \tag{22}$$

Peak-to-peak current ripple is:

$$\Delta I_{in} = k_{in}\delta T \tag{23}$$

Following procedure outlined in 2.1, the value of current ripple for δ<1/3 is derived as:

$$\Delta I_{in} = \delta(1 - 3\delta)\frac{V_{out}T}{L_{in}} \tag{24}$$

- **1/3<δ<2/3**

Figure 20 illustrates input current waveforms for 1/3<δ<2/3.

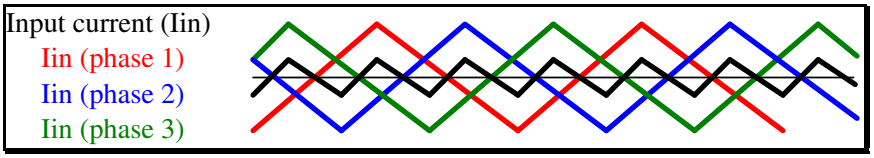

Fig. 20. Three-phase boost converter - input current waveforms, 1/3<δ<2/3

In this case the input current's rising slope duration is (δ-1/3)T and the value is

$$k_{in} = 2k_{on} - k_{off} = 2\frac{V_{in}}{L_{in}} - \frac{(V_{out} - V_{in})}{L_{in}} \tag{25}$$

Input current ripple is:

$$\Delta I_{in} = k_{in}(\delta - \frac{1}{3})T = \left(\delta - \frac{1}{3}\right)(2 - 3\delta)\frac{V_{out}T}{L_{in}} \tag{26}$$

- **δ>2/3**

Figure 21 illustrates input current waveforms for δ>2/3.

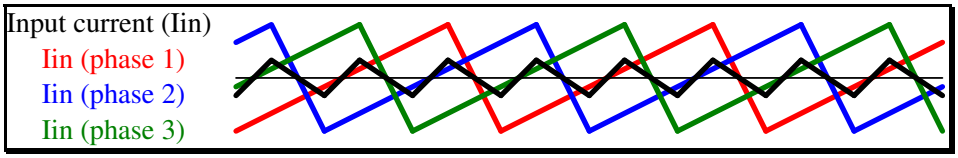

Fig. 21. Three-phase boost converter - input current waveforms, δ>2/3

The input current ripple slope duration is (δ-2/3)T and

$$k_{in} = 3k_{on} = 3\frac{V_{in}}{L_{in}} \tag{27}$$

$$\Delta I_{in} = k_{in}(\delta - \frac{2}{3})T = \left(\delta - \frac{2}{3}\right)(3 - 3\delta)\frac{V_{out}T}{L_{in}} \tag{28}$$

3.3.2 Output capacitor RMS current

- δ<1/3

  Figure 22 illustrates filter capacitor current for δ<2/3.

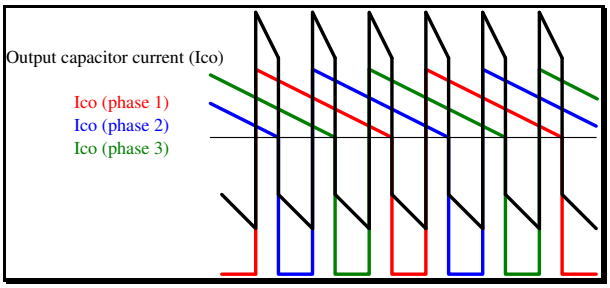

Fig. 22. Three-phase boost converter - output capacitor current waveform, δ<1/3

- Positive amplitude: (I_{inAVG}-I_{out}), duration: (1/3 - δ)T
- Negative amplitude: (I_{out}-2I_{inAVG}/3), duration: δT

  RMS current:

$$I_{CoRMS}^2 = \delta\left(I_{out} - \frac{2}{3}I_{inAVG}\right)^2 + \left(\frac{1}{3} - \delta\right)\left(I_{inAVG} - I_{out}\right)^2 \tag{29}$$

$$I_{CoRMS} = \frac{I_{out}}{3(1-\delta)}\sqrt{\delta(1-3\delta)} \tag{30}$$

- **1/3<δ<2/3**

  Figure 23 illustrates filter capacitor current for 1/3<δ<2/3.

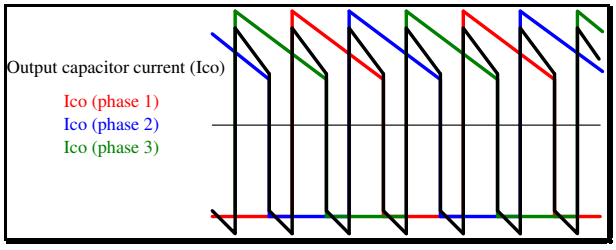

Fig. 23. Three-phase boost converter - output capacitor current waveform, 1/3<δ<2/3

- Positive amplitude: ($2I_{inAVG}/3 - I_{out}$), duration: $(2/3-\delta)T$
- Negative amplitude: ($I_{out} - I_{inAVG}/3$), duration: $(\delta-1/3)T$
  RMS current:

$$I_{CoRMS}^2 = \left(\delta - \frac{1}{3}\right)\left(I_{out} - \frac{1}{3}I_{inAVG}\right)^2 + \left(\frac{2}{3} - \delta\right)\left(\frac{2}{3}I_{inAVG} - I_{out}\right)^2 \quad (31)$$

$$I_{CoRMS} = \frac{I_{out}}{3(1-\delta)}\sqrt{\frac{1}{3}(3\delta-1)(2-3\delta)} \quad (32)$$

- **δ>2/3**
  Figure 24 illustrates filter capacitor current for $\delta>2/3$.

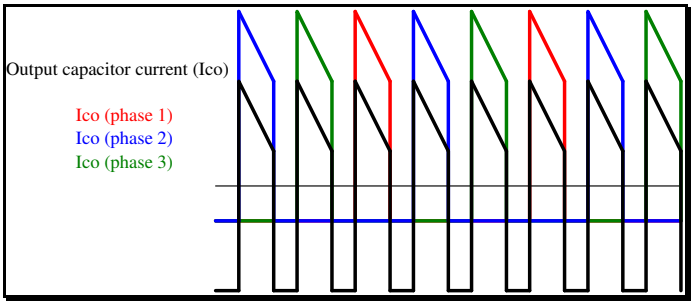

Fig. 24. Three-phase boost converter - output capacitor current waveform, $\delta>2/3$

- Positive amplitude: ($I_{inAVG}/3 - I_{out}$), duration: $(1-\delta)T$
- Negative amplitude: I_{out}, duration: $(\delta - 2/3)T$
  RMS current:

$$I_{CoRMS}^2 = \left(\delta - \frac{2}{3}\right)I_{out}^2 + (1-\delta)\left(\frac{1}{3}I_{inAVG} - I_{out}\right)^2 \quad (33)$$

$$I_{CoRMS} = \frac{I_{out}}{3(1-\delta)}\sqrt{\frac{1}{3}(3\delta-2)(3-3\delta)} \quad (34)$$

3.4 Generalization for n phases

3.4.1 Input current ripple

All the results obtained in the previous sections are summarized in the table below. Equations for the 4-phase boost converters are added to the table as they will be used in the following sections. Finally, the general forms of the equations for an n-phase converter are listed in the last row.

Having all relevant equations in one place makes it easy to illustrate benefits of interleaving by graphing input current ripple vs. duty cycle.

Figure 25 shows normalized graphs of the input current ripple for 1, 2, 3 and 4-phase boost converters as a function of duty cycle.

Number of phases (n)	Interval 1 $\delta<1/n$	Interval 2 $1/n<\delta<2/n$	Interval 3 $2/n<\delta<3/n$	Interval 4 $3/n<\delta<4/n$	....	Interval i $(i-1)/n<\delta<i/$
1	$\delta(1-\delta)\frac{V_{out}T}{L_{in}}$					
2	$\delta(1-2\delta)\frac{V_{out}T}{L_{in}}$	$\left(\delta-\frac{1}{2}\right)(2-2\delta)\frac{V_{out}T}{L_{in}}$				
3	$\delta(1-3\delta)\frac{V_{out}T}{L_{in}}$	$\left(\delta-\frac{1}{3}\right)(2-3\delta)\frac{V_{out}T}{L_{in}}$	$\left(\delta-\frac{2}{3}\right)(3-3\delta)\frac{V_{out}T}{L_{in}}$			
4	$\delta(1-4\delta)\frac{V_{out}T}{L_{in}}$	$(\delta-\frac{1}{4})(2-4\delta)\frac{V_{out}T}{L_{in}}$	$(\delta-\frac{2}{4})(3-4\delta)\frac{V_{out}T}{L_{in}}$	$(\delta-\frac{3}{4})(4-4\delta)\frac{V_{out}T}{L_{in}}$		
…	….	….	….	….	….	
n	$\delta(1-n\delta)\frac{V_{out}T}{L_{in}}$	$(\delta-\frac{1}{n})(2-n\delta)\frac{V_{out}T}{L_{in}}$	$(\delta-\frac{2}{n})(3-n\delta)\frac{V_{out}T}{L_{in}}$	$(\delta-\frac{3}{n})(4-n\delta)\frac{V_{out}T}{L_{in}}$	....	$\left(\delta-\frac{i-1}{n}\right)(i-n\delta)$

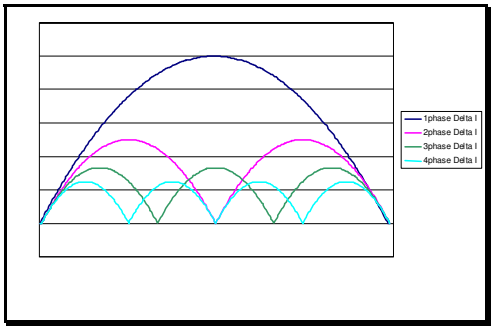

Fig. 25. Input current ripple current vs. duty cycle

The effects of multiphase converters become clearly visible as the maximum current ripple becomes progressively smaller and ripple cancellation effects occur (n-1) times (n being the number of phases). Note that duty cycles of zero (0) and one (1.0) are of theoretical value only and ripple cancellation at those duty cycles is of no practical consequence.
Peak value of the ripple current can be found by searching for the maximum of the function for n phases and interval 1 (in the table above):

$$\Delta I_{in} = \delta\left(1 - n\delta\right)\frac{V_{out}T}{L_{in}} \tag{35}$$

The maximum is then found as:

$$\Delta I_{in(\max)} = \frac{1}{4n}\frac{V_{out}T}{L_{in}} \tag{36}$$

Normalized graphical representation of Eq (36) is simple and shown in Figure 26.

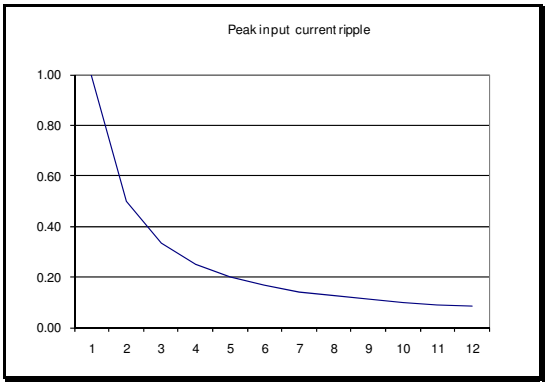

Fig. 26. Peak input current ripple vs. number of phases

3.4.2 Output capacitor RMS current

The results for the closed form equations are sorted in the table below. The table is expanded to show 4-phase inverter equations and the general case of an n-phase boost converter.

Number of phases (n)	Interval 1 $\delta<1/n$	Interval 2 $1/n<\delta<2/n$	Interval 3 $2/n<\delta<3/n$	Interval 4 $3/n<\delta<4/n$	....	Interv $(i-1)/n<$
1	$\frac{I_{out}}{(1-\delta)}\sqrt{\delta(1-\delta)}$					
2	$\frac{I_{out}}{2(1-\delta)}\sqrt{\delta(1-\delta)}$	$\frac{I_{out}}{2(1-\delta)}\sqrt{\frac{1}{2}(2\delta-1)(2-2\delta)}$				
3	$\frac{I_{out}}{3(1-\delta)}\sqrt{\delta(1-3\delta)}$	$\frac{I_{out}}{3(1-\delta)}\sqrt{\frac{1}{3}(3\delta-1)(2-3\delta)}$	$\frac{I_{out}}{3(1-\delta)}\sqrt{\frac{1}{3}(3\delta-2)(3-3\delta)}$			
4	$\frac{I_{out}}{4(1-\delta)}\sqrt{\delta(1-4\delta)}$	$\frac{I_{out}}{4(1-\delta)}\sqrt{\frac{1}{4}(4\delta-1)(2-4\delta)}$	$\frac{I_{out}}{4(1-\delta)}\sqrt{\frac{1}{4}(4\delta-2)(3-4\delta)}$	$\frac{I_{out}}{4(1-\delta)}\sqrt{\frac{1}{4}(4\delta-3)(4-4\delta)}$		
…	….	….	….	….	….	
n	$\frac{I_{out}}{n(1-\delta)}\sqrt{\delta(1-n\delta)}$	$\frac{I_{out}}{n(1-\delta)}\sqrt{\frac{1}{n}(n\delta-1)(2-n\delta)}$	$\frac{I_{out}}{n(1-\delta)}\sqrt{\frac{1}{n}(n\delta-2)(3-n\delta)}$	$\frac{I_{out}}{n(1-\delta)}\sqrt{\frac{1}{n}(n\delta-3)(4-n\delta)}$	….	$\frac{I_{out}}{n(1-\delta)}\sqrt{\frac{1}{n}(n\delta$

Figure 27 shows graphs of the normalized RMS current for 1, 2, 3 and 4-phase boost converters as a function of duty cycle.

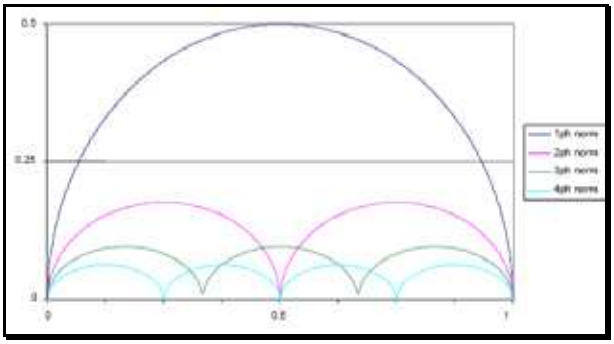

Fig. 27. Normalized output capacitor RMS current vs. duty cycle

The ripple cancellation effects are also very pronounced, but it should be noted once again that, on the output capacitors, there is no complete cancellation - there is always a ripple current present. In our analysis the inductor ripple current was neglected. Even though it is relatively small it never cancels at the output and zero values in Figure 27 should be considered points with the minimum, not zero, ripple.
Peak value of the ripple current can again be found by searching for the maximum of the function for n phases and interval 1 (in the table above):

$$I_{CoRMS} = \frac{I_{out}}{n(1-\delta)}\sqrt{\delta(1-n\delta)} \tag{37}$$

The peak RMS current (maximum of the function represented by Eq 37 is then found as

$$I_{CoRMS(\max)} = \frac{I_{out}}{(2n-1)\sqrt{n}} \tag{38}$$

Normalized graphical representation of Eq (38) is shown in Figure 28

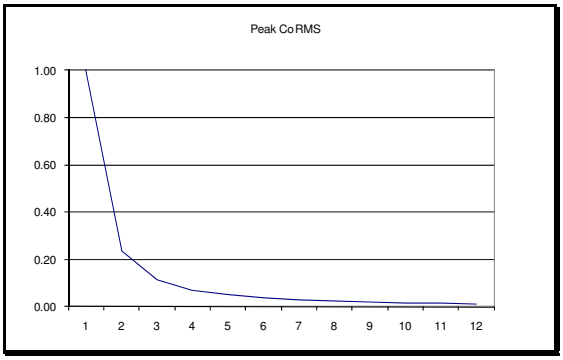

Fig. 28. Normalized output capacitor RMS current vs. number of phases

It is interesting to see effects of multiple phases on reduction of peak inductor and capacitor currents, when normalized to the same value. Such interpretation is shown in Figure 29.

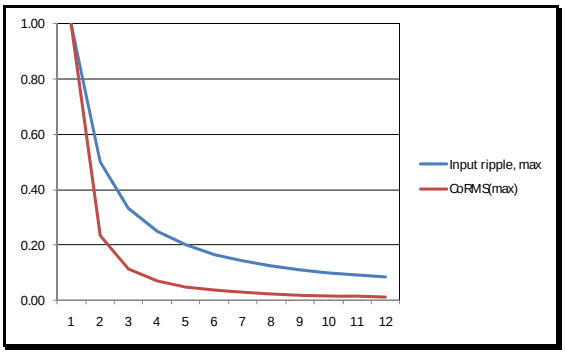

Fig. 29. Comparison of normalized capacitor and inductor (input) current

Capacitor RMS current gets reduced faster as the number of phases in an interleaved converter increases. This is a very good news indeed, as capacitors represent one of the components with shortest life time. Most components typically used in a power train have life span that measures in tens or even hundreds of thousands of hours, and electrolytic capacitors have life expectation of well below 10000 hours under full load.

4. Optimizing number of phases

Figure 29 as previously derived (and, for convenience, copied below as Figure 30) can serve as an indication that arbitrary increase of the number of phases in an interleaved configuration may quickly invoke the law of diminishing returns, starting with relatively low number of phases.

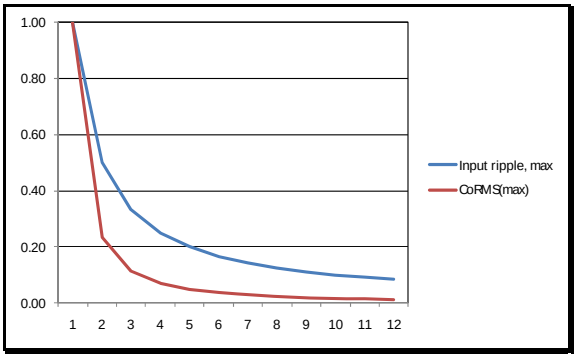

Fig. 30. Comparison of normalized capacitor and inductor (input) current

The process of selection of the number of phases has not been adequately addressed in literature. Most of the time it is selected as a compromise between benefits of an interleaved design and increased cost and complexity. Two phase designs are starting to be popular in PFC designs, although their wide acceptance is yet to be seen.

However, taking a closer look into design requirements and utilizing work done in previous sections can help illustrate a simple optimization method applicable in practice. Understanding the application and specific requirements outlined in Chapter 2.1 proves to be crucial.

4.1 "Real World" operating condition

A good specification is designed to cover all possible operating conditions and adds small margins to ensure safety and reliability. Such specification assigns equal importance to all listed parameters over the whole specified range. Optimization for an infinite number of operating points is often impossible. Luckily, considering actual, "real world" operating conditions, it can be seen that the list of critical parameters and their ranges indicate much narrower operating conditions, and chances of successful optimization are much greater. The "real world" conditions, in the context of this work, are considered operating parameters where converter works most of the time - in other words, this would be an average loading if extreme peak loads (that are infrequent and short in duration) are neglected. For example – even though input voltage range is specified 24-36V, converter will see steady input voltage of 28V during normal operation. It is understood that the regulator must operate within specifications over full operating range, but it still makes a lot of sense to optimize critical parameters for a situation that will apply for most of the unit's serviceable life. Minimizing output capacitor ripple for "real world" operating point will extend their life and life of the unit. Optimum efficiency will result in less heat and smaller, less expensive thermal design.

Chapter 2.1, Specification requirements, lists that the 5kW boost converter used as a fuel cell voltage regulator needs to operate over the following voltage ranges:

- Input voltage range: 24-36V
- Output voltage range: 37-60V

Starting with the equation for the boost converter DC gain (Eq 4) it is easy to calculate that such a converter will operate over an extremely wide duty cycle between 0.03 and 0.6. This is a nominal duty cycle range. Designing the converter to cover this wide range at full power would present a challenge regarding driver circuits and containment of electromagnetic emissions.

Considering positive impact of interleaving it is obvious that higher number of phases will help reduce input current ripple as well as the output capacitor's RMS current. Due to the very wide operating range it is not easy to qualify those perceived benefits. A closer look at the application and converter's operating conditions is a necessary step toward circuit optimization:

Wide input voltage range: 24V is the fuel cell's "knee" voltage (Region of Concentration Polarization in Figure 31 below) - the fuel cell is in overload and output impedance is rising sharply. Clearly, this is not normal operation, as the system's current limits need to protect both the fuel cell and the regulator. On the other side of the range, 36V is the fuel cell's no-load (ideal) voltage and the only practical implication is ensuring that the voltage ratings of the associated equipment are adequately selected. In normal steady-state operation the output voltage varies very little and is typically around 28V.

Wide output voltage range: the actual system operates with 36V batteries and the 40-60V range is specified for possible future expansion to 48V system. In the 36V system, the converter's output voltage is set to keep batteries charged to 41V (slightly below the fully charged level to ensure that batteries can absorb recuperative braking energy). Therefore,

41V is the output voltage that will be maintained for all operating conditions except for peak loads that exceed 5.5kW rating of the regulator.

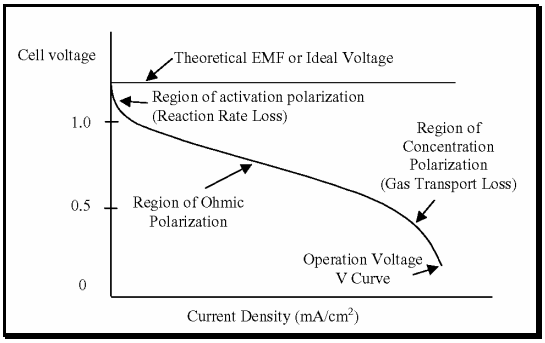

Fig. 31. A typical fuel cell load curve

4.2 Optimization

With the practical considerations listed above, the regulator's operating point is:

- Input voltage: 28V
- Output voltage: 41V
- Operating duty cycle: 0.32

A useful visual representation can be obtained by starting with normalized graphs (ΔIin and I_{CoRMS} vs. duty cycle) and superimposing nominal and operating duty cycles.

Figure 32 shows normalized input ripple current with nominal duty cycle range (0.03-0.60) and operating range (centered around δ=0.32) superimposed. Figure 33 shows normalized output capacitor ripple current and nominal and operating duty cycles.

Contrary to the generalized statement that current levels decrease with the number of interleaved phases, examination of Figures 32 and 33, considering a narrow duty cycle range centered around 0.32 shows that the input current ripple, as well as the output capacitor RMS current are significantly lower in the three-phase design than in the higher order, four phase design. Counterintuitive on the first sight, but easily understood considering that operating duty cycle is located very close to the zero-current duty cycle. Therefore, for the real-life, application specific operating conditions the three-phase interleaved converter offers significant benefits compared to the four-phase design: it yields lower cost unit with reduced complexity and, at the same time, results in the lower stress of the output capacitors and, quite likely, lower emissions as a result of reduced input current ripple.

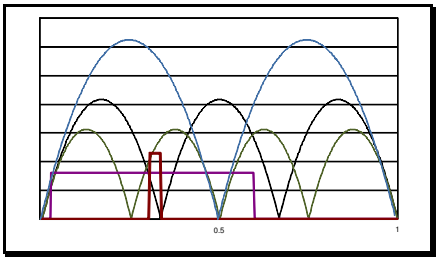

Fig. 32. Input current ripple with nominal and operating duty cycle

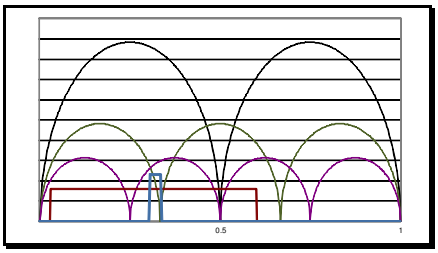

Fig. 33. Output capacitor RMS current with nominal and operating duty cycle

During certain events - system start, initial battery charging, overvoltage or overload transients, the converter will work over the much wider range of input and output voltages, departing from this narrowly defined area. During those events, the converter will work in a suboptimal mode. However, those events are rare (overvoltage conditions are an abnormal situation, system starts once per work shift and the initial battery charging is done only when a new system is initialized) and short in duration (system start is in ~30 seconds, initial battery charging is ~ 1hr or less, overload transients may last few seconds). As such, these still regular but suboptimal modes of operation will not overstress the unit for any significant amount of time that would significantly reduce the regulator's service life.

5. Regulator design

At this point the electrical specification and application requirements are known (Chapter 4) and three phase interleaved boost converter was proven to be optimum topology for the application. Next step is regulator design, which can be divide into two major sections – power stage and control section.

5.1 Power stage

Simplified representation of the three-phase boost converter power stage is shown in Fig. 34.

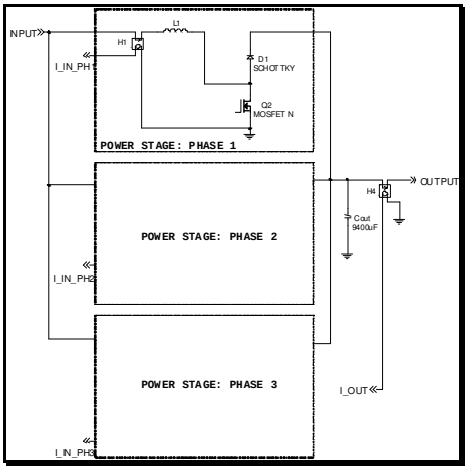

Fig. 34. Block schematic of the three phase boost converter

The concept is identical to the basic topology shown in Figure 34, but this representation adds more details. Input current is measured at each phase in order to ensure current sharing. Output current is also measured in order to provide accurate monitoring and battery charging.

5.2 Switching frequency selection

Electromagnetic compatibility (EMC) issues are typically addressed at the end of a design cycle, when components selection, board layout and mechanical packaging are finalized. However, keeping in mind the EMC at the very beginning of a design pays large dividends when the finalized product is submitted for radiated and conductive emissions testing. Switching frequency was selected based on minimal anticipated electromagnetic emissions. Alternative approach could be starting with efficiency requirements and losses, but it requires that all components are selected which limits options early in the design.

Input inductor current has a triangular ac component (high frequency ripple). Most of the other waveforms have shapes that include part of a triangle. It is not surprising, therefore, that third harmonic is typically the most dominant in the electromagnetic spectrum of a power converter.

Two major groups of standards dominate regulations of the emissions that can be tolerated. FCC, part 15 is mandatory in the US and EMC Directive (required in order for units to carry the CE mark) must be complied with in European Union and many other countries (notably Japan, Australia and China). The emission limits dictated by FCC and CE are very similar, major difference being that FCC limits start at 450kHz, while CE limits start at a lower frequency – 150 kHz. Meeting CE requirements automatically means complying with FCC as well.

Safe approach to selecting switching frequency is to ensure that the most dominant third harmonic of the switching frequency falls just at or slightly below the frequency that matters for certification. For CE compliance, the frequency of the third harmonic should, therefore, be 150 kHz, which automatically yields maximum switching frequency of 50kHz, or 16.6kHz per phase.

Unfortunately, 16.6kHz falls into the audible range and using this frequency may not be ergonomically feasible. As a compromise, the 25kHz is chosen for the final application as it is not audible and still it seems to be far enough below the mandated test frequency of 150kHz. Since the initial production is planned for the US market where FCC rules apply (minimum frequency is 450kHz which is the 6^{th} harmonic of our switching frequency, therefore not critical) the we can be reasonably confident in meeting the required specs without major modifications at the time of regulatory approvals.

5.3 Inductor design

Compact high power inductors are difficult to make without specialized equipment. Many manufacturers also offer design services. However, it is still beneficial to go through initial parts of the design in order to define basic inductor parameters to ensure that the final design makes perfect sense for the application.

Requirements for small size dictate use of powder cores. There are many variations available, from iron powder, MPP, Cool μ, etc. each with slightly different characteristics and optimum use.

Considering price and availability in the adequate core size, iron powder cores offer the widest selection. This type of core is available at lowest cost, however, it suffers from

thermal aging problem. If exposed to increased operating temperature, over time its permeability drops and losses increase causing potentially hazardous situations.
Fortunately, new materials were recently developed, enabling operation of up to 200°C which increase capabilities beyond those possible even with ferrite cores. Those are *200C Series High Temperature Powder Cores* from Micrometals.
Material designated as -60 was among the first ones available in wide spectrum of shapes and sizes, and it was chosen for our design. For anyone with experience in designing with powder cores, the process is straightforward. Thanks to soft saturation characteristics of powder cores, high accuracy and numerous iterations requiring optimization are not required. This type of cores typically operates in the saturation region where permeability drops to 30-70% of the initial permeability.
The design starts with finding worst case average inductor current (I_{Lin}):

$$I_{in} = \frac{P_{out}}{\eta V_{in(\min)}} = \frac{5500W}{0.96 \cdot 24V} = 239A \tag{39}$$

Output power (P_{out}), efficiency (η) and minimum input voltage ($V_{in(min)}$) are input data defined in the electrical specification.
In the three phase design, each input inductor will see 1/3 of the total input current, or I_L=80A.
Considering ripple attenuation effects, allowable worst case inductor current ripple can be selected as 30% of the average inductor current, for ΔI_L=24A. Peak inductor current I_{Lpk} is then

$$I_{Lpk} = I_L + \frac{\Delta I_L}{2} = 92A \tag{40}$$

$$\Delta I_L = \frac{V_{in(\min)}\delta}{f_{sw}L} \Rightarrow L = \frac{V_{in(\min)}\delta}{f_{sw}\Delta I_L} \tag{41}$$

Switching frequency (f_{sw}) is 25kHz and worst case duty cycle (δ) was calculated as 0.6. Therefore, inductance of the input inductor is calculated as

$$L=24\mu H$$

Material -60 was the only 200°C material available without long wait times. This is material designed for most common application and can be used in variety of applications, hence wide range of available core sizes. For our design an E305-60 core was selected. The main parameters of the core are:

- Initial (reference) permeability μ=55
- Inductance factor A_L=222 nH/N²
- Equivalent length of magnetic path l_e=18.5 cm
- Equivalent cross section A_e=5.62 cm²
- Equivalent core volume V_e=139 cm³

Initial number of turns (N_i) is calculated as

$$N_i = \sqrt{\frac{L}{A_l}} = 10.4\ turns \tag{42}$$

The initial number of turns will later be corrected to account for partial saturation of the core, so it may stay as the decimal number, rather than being rounded up.
Owing to the fact that all major iron powder core manufacturers come from the USA, size parameters and material characteristics are given in the CGS units of measure, rather than in the SI units – cm instead of m, Öersted (Öe) instead of A/m, Gauss (G) instead of Tesla (T), etc. Even though equations get to be little more cumbersome, in the end it is easier to work with them than to make double conversions.
Magnetizing force is calculated next:

$$H = \frac{0.4\pi N_i I_{Lpk}}{l_e} \tag{43}$$

Substituting previously listed and calculated values yields magnetizing force

$$H=65\ Öe$$

Figure 35 details soft saturation characteristics of 200°C iron powder cores. Permeability change (in %) is given as function of magnetizing force.

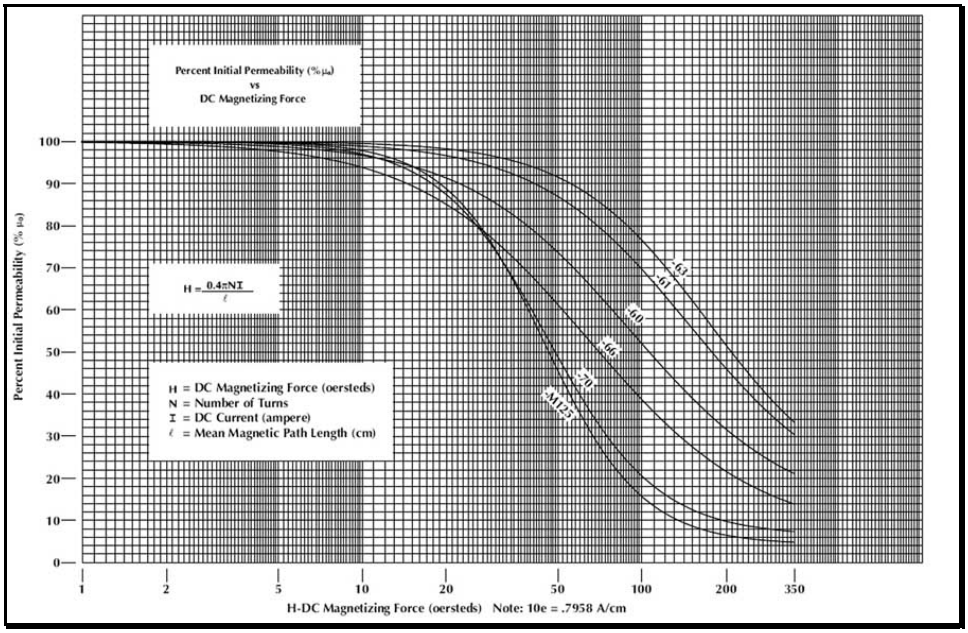

Fig. 35. Permeability change vs. magnetizing force

For magnetizing force of 65 Öe permeability of -60 material will drop to 66% of the initial permeability. In order to compensate for drop in permeability, initial number of turns N_i needs to be corrected to get final number of turns N:

$$N = \frac{N_i}{0.66} = 15.76\ turns, \textit{ rounded up to } 16\ turns \tag{44}$$

In order to confirm feasibility of the selected core, a quick look at losses is required. Based on similar size cores for which the information is available, thermal resistance for this core can be estimated at R_Θ = 1.5 °C/W (assuming some air is being circulated around the inductors). Considering maximum operating ambient of 60°C, there is about 70°C of temperature rise before inductors become too hot for quick safety approvals. Considering the above, our power loss budget is about 47W per inductor.
Two main components of inductor loss are core loss and copper loss (in the windings). Core loss is easy to find from the graph showing core loss versus flux density (Figure 36).

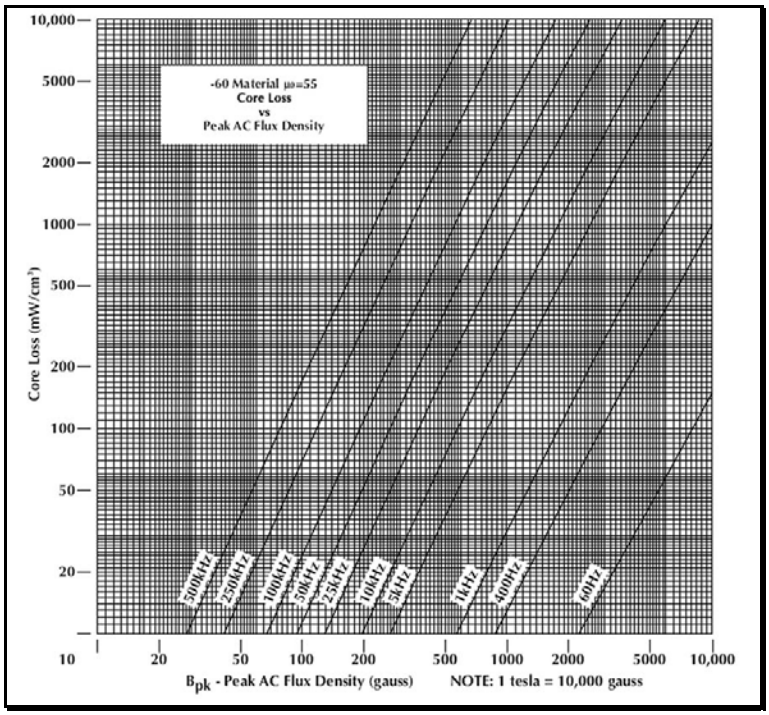

Fig. 36. Specific core loss vs. flux density

In our design, worst case peak flux density is calculated as

$$B_{pk} = \frac{V_{in}\,\delta}{f_{sw}\,A_e\,N} \tag{45}$$

Worst case, high power operation will occur when input voltage is V_{in}=24V, output voltage V_{out}=41V and resulting duty cycle δ=0.41. substituting these values into Equation 45 will yield peak flux density of B_{pk} = 44mT = 440G.
At switching frequency of 25kHz, specific core loss is about 180 mW/cm³. Considering core volume of 139 cm³, the core loss comes to 25W. With total power loss budget of 47W and core loss of 25W, copper loss can be as high as 22W. Reviewing the numbers, the core loss and copper loss are close which indicates adequate inductor design (very often the starting goal in a magnetic design is to make core loss equal to the copper loss).

Information regarding core type and size, number of turns and power budget was relayed to inductor manufacturer who designs windings based on available conductor type (wire of foil) suitable for their manufacturing process. Photograph of the finished inductor is shown in Figure 37.

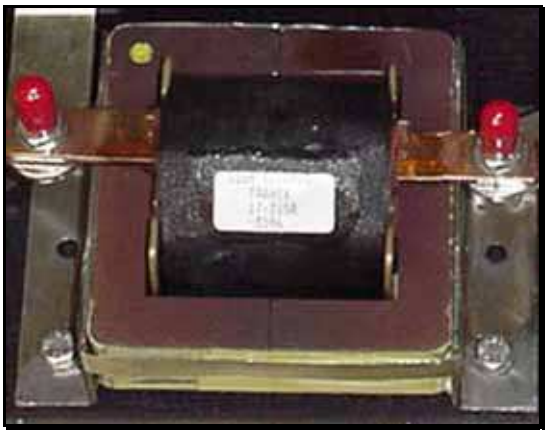

Fig. 37. **Photo of the finished input inductor**

5.4 Power switch selection

Power MOSFETs are the most suitable parts to be used as high frequency switches, thanks to their high switching speed, low cost and low losses. High current MOSFETs are readily available. In high power designs, MOSFET selection needs to be done based on design's ability to dissipate heat generated due to power loss. Switch current waveform is shown in Figure 38.

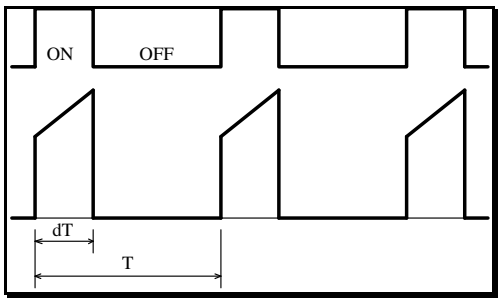

Fig. 38. Switch current waveform

RMS current through the switch in one phase can be calculated as:

$$I_{sw(RMS)} = \frac{I_{out}}{1-\delta}\sqrt{\delta\left(1+\frac{(\Delta I_L/I_L)^2}{12}\right)} \tag{46}$$

Substituting worst case situation as determined for input inductor calculations I_{out}=150A/3 (per phase), ΔI_L=24A, I_L=80A and δ=0.41, switch RMS current is found to be

$$I_{sw(RMS)} = 55A$$

Low input voltage and low switching frequency indicate that switching loss in power MOSFETs is going to be negligible when compared to the conduction loss due to the high RMS current and $R_{ds(ON)}$ characteristic of the part. MOSFET channel resistance, $R_{ds(ON)}$ is the parameter we can use in order to minimize the loss in the converter switch.
In order to ensure good thermal management, it was decided to use multiple components in parallel in order to spread generated heat over larger equivalent cooling area. Surface mounted components make it possible to use automated assembly and significantly reduce manufacturing time and errors. D²PAK package, shown in Figure 39 proves to be optimal for the application.

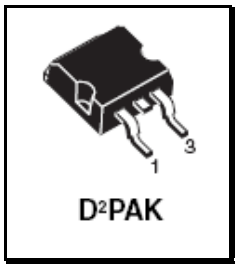

Fig. 39. D2PAK package

After close examination of several usable MOSFETs from International Rectifier, Fairchild Semiconductor, Vishay and ST Microelectronics, an ST part STB160N75F3 was chosen for the application thanks to its low $R_{ds(ON)}$ and input capacitance, fast turn-on and turn-off, high maximum operating temperature, low cost and availability on the market. Critical specifications for the MOSFET are:

- Open channel resistance: $R_{ds(ON)25}$ = 3.7mΩ max (at 25°C)
- Maximum drain-source voltage: V_{DS} = 75V
- Maximum drain current: I_D = 120A (limited by package)
- Input capacitance: C_{iss} = 6750pF
- Maximum operating junction temperature: T_j = 175°C

MOSFETs have positive temperature coefficient, indicating that $R_{ds(ON)}$ increases with temperature. For STB160N75F3, normalized ON resistance change with temperature is shown in Figure 40.
In order to comply with safety requirements, thermal design will need to ensure that maximum component temperature does not exceed 105°C. Junction temperature can be estimated to be approximately 20° higher. Assuming junction temperature of 125°C, actual operating $R_{ds(ON)}$ will be 1.7 times higher than at 25°C. Therefore, for loss calculations

$$R_{ds(ON)} = 1.7\ R_{ds(ON)25} = 6.3m\Omega$$

Assuming only one MOSFET per phase, conduction loss would be

$$P_c = R_{ds(ON)}\, I_{sw(RMS)}^2 = 0.0063 \cdot 55^2 = 19\ W$$

This seems excessive considering size of the package and need to dissipate the power in high ambient temperature. In order to keep dissipation per MOSFET low and converter efficiency high, it was decided to use six (6) MOSFETS in parallel for each phase.

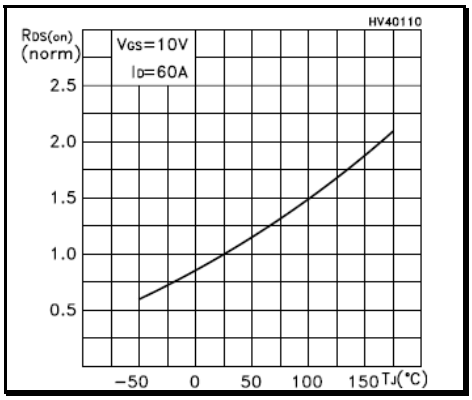

Fig. 40. Normalized ON resistance vs. temperature

5.5 Rectifier selection

Reverse recovery time of a diode rectifier is major contributor to power loss in the boost converter's power switch. That loss is directly proportional to switching frequency. Low switching frequency here helps minimize this type of loss. To practically eliminate the loss, Schottky diodes can be used. They will also minimize loss in the diode rectifier.

Average current through the boost rectifier is equal to the load current. Maximum load current is specified as 150A. Split between three phases will yield 50A per phase. In order to ensure healthy margin in the design a 100V Schottky diode from ST Microelectronics was selected. Package is again D²PAK, part number is STPS30SM100S and the most important specifications for the diode are:

- Repetitive peak reverse voltage: V_{RRM} = 100V
- Average forward current (δ=0.5): $I_{F(AV)}$ = 30A
- Forward voltage drop (I_F=10A and T_j=125°C): V_F = 560mV
- Maximum operating junction temperature: T_j = 175°C

In order to ensure adequate cooling with sufficient margins for asymmetrical current sharing, six (6) diodes will be used in parallel. Total power loss per phase can be estimated as

$$P_d = V_F \cdot I_{out}/3 = 0.56 \cdot 150/3 = 28W$$

Diode loss is much higher than MOSFET loss and will be major contributor to overall losses. However, at less than 5W per diode, in worst case operating conditions, it will be easily manageable.

5.6 Output capacitors

Output filter capacitors are selected based on two criteria: (1) allowable high frequency output voltage ripple at maximum load determines acceptable minimum capacitance and (2) maximum capacitor RMS current determines type and number of capacitors used. Very often this second criteria drives the capacitor selection and minimum capacitance is easier to achieve with modern parts.

Equation 38 defines maximum capacitor RMS current as

$$I_{CoRMS(\max)} = \frac{I_{out}}{(2n-1)\sqrt{n}} \tag{38}$$

Output current, I_{out} = 150A
Number of interleaved phases n = 3

$$I_{CoRMS(max)} = 17.3\ A$$

The hybrid fuel cell system has lead-acid battery connected at the output and it will help smooth the ripple at high loads. The main concern is, therefore current handling capacity of the output capacitors.
Aluminum electrolytic capacitors VZ series from Nichicon offer low profile, reasonably price and 10000 hours life at 105°C temperature rating.
Value of 470µF/63V has rated RMS current of 640mA at 120Hz. Typically, at higher frequencies capacitor current rating increases and for this capacitor and above 10kHz, frequency multiplier is specified as 1.5, resulting in capacitor's current rating of 960mA.
In order to satisfy worst case RMS current of 17.3A we need minimum of 18 capacitors.
Control circuit, as the name implies, ensures optimum driving of the power stage and provides protections and communications with the outside world. It has the following functions:

- Generation of interleaved PWM signals and MOSFET drivers
- Ensuring stable operation and current sharing between the phases
- Communication with the fuel cell system controller
- Protections:
  - Output current limit
  - Overvoltage protection
  - Reverse current protection
  - Overload protection
  - Thermal protection

6 Interleaved PWM signals

In recent years some dedicated controllers were developed for multiphase applications. Advantages of a highly integrated solution are in simplicity, reliability and shorter development. Disadvantages are that these converters are developed for very specific applications such as PFC or low voltage converters, operation at very high frequencies, lack of flexibility and uncertain future of the part – most semiconductor manufacturers have habit of discontinuing parts if they do not meet sales projections. In other words, if the part does not get designed in a high volume product that results in sales of few million pieces, it is likely that it will be discontinued and replaced with something else. This is the risk that is unacceptable for industrial products that have design life of 10 years or more and being unable to find parts results in very costly redesigns.
Instead of using a dedicated multiphase controller, a safer solution, standard, readily available PWM controller was selected. UCC2581 from Texas Instruments has all the functions that are required. There will be one controller used per phase.
UCC2581 controller has SYNC input, which can be used to synchronize several controllers in order to help reduce EMI. In this application the controller is synchronized to one output of the simple three phase oscillator as shown in the block diagram, Figure 41.

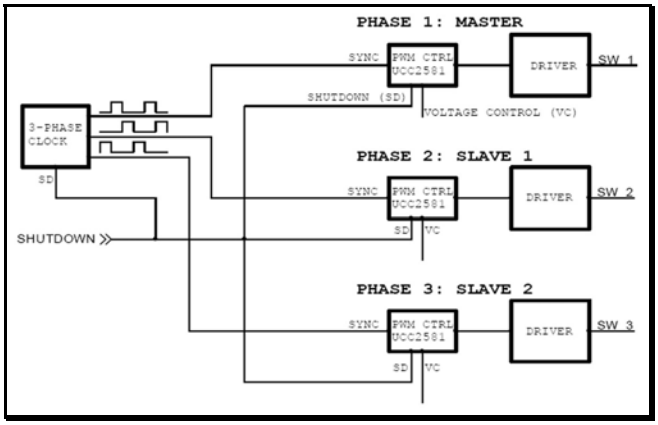

Fig. 41. PWM control block diagram

Another aspect of control can also be seen from the block diagram – current sharing between the three phases will be actively managed in master-slave configuration. In this arrangement, master phase is set to maintain the output voltage regulation and slave phases are designed to closely follow input current of the master slave. This ensures that all three input inductors operate with the same input current, regardless of the load conditions. Even though not the simplest method, the master-slave current sharing offers the most accurate load distribution. Load sharing to within 1% can typically be expected. This is especially important in high power design where over-rating components carries significant price tag. Schematics of the three phase oscillator is shown in Figure 42.

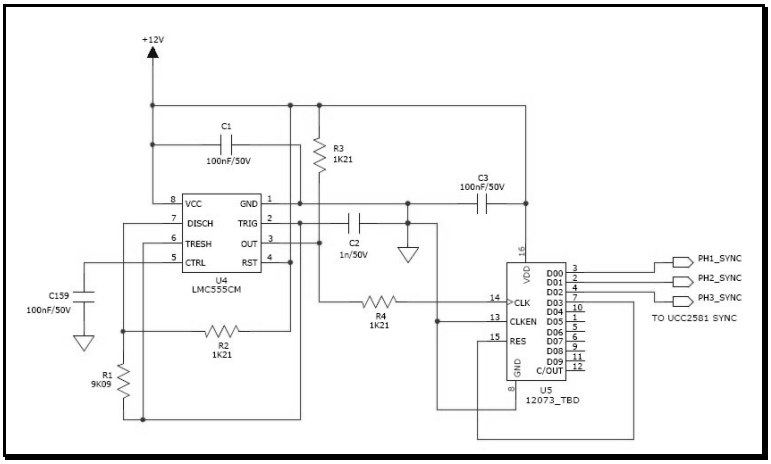

Fig. 42. Schematics of the three phase oscillator

The three SYNC outputs are spaced at 120° and fed to their respective PWM controllers. This not only synchronizes switching frequencies of the three phases but also interleaves driving pulses equally distributing them over the full switching period. Schematics of an implemented PWM controller is shown in Figure 43.

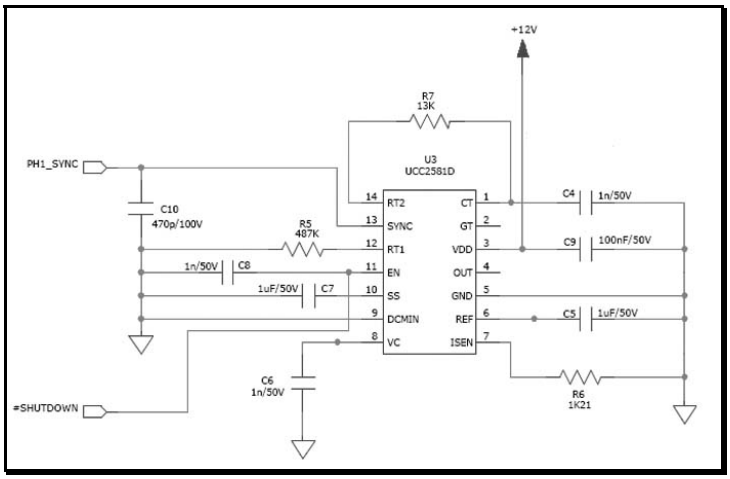

Fig. 43. PWM controller schematics

PWM controller output is fed to a MOSFET driver in order to ensure adequate drive and fast transitions during turn on and turn off of the MOSFETs.

6.1 Control strategy

Negative feedback (NFB) loop ensures stable operation of the fuel cell regulator over the full range of operating conditions. For effective control of the fuel cell system, the following variables need to be controlled:

- Output voltage (needs to be adjustable)
- Input current (this is fuel cell output current and also needs to be adjustable)
- Output current (current limit – when the output current reaches certain level, above normal operating current, the regulator needs to switch to the constant current mode operation)
- Current sharing (in master-slave configuration, as previously mentioned, slave phases need to closely follow input current of the master phase).

Every parameter requires its own NFB loop and there will be several error amplifiers (E/A), as illustrated by Figure 44.

Master error amplifiers (E/A) respond to control signal for input current and output voltage (analog inputs). Their outputs are OR-ed together to ensure that, at any point in time, only one error amplifier is controlling the operation, and that is an error amplifier with the lowest output (error) voltage. Third error amplifier (lowest one in Figure 44) sets output current limit and has fixed reference signal. If the output current reaches preset value defined by the reference voltage REF-I_OUT_MAX, its output will become the lowest of the three and output current will be kept constant regardless of the other two variables (ANALOG_I_IN_CTRL and ANALOG_V_OUT_CTRL)

Input current of the master phase is fed as a reference to the two error amplifiers controlling input current of the slave phases (top two E/A Figure 44). Error voltage of the slave E/A becomes control voltage for the slave phases and that ensures very accurate current sharing among all three phases.

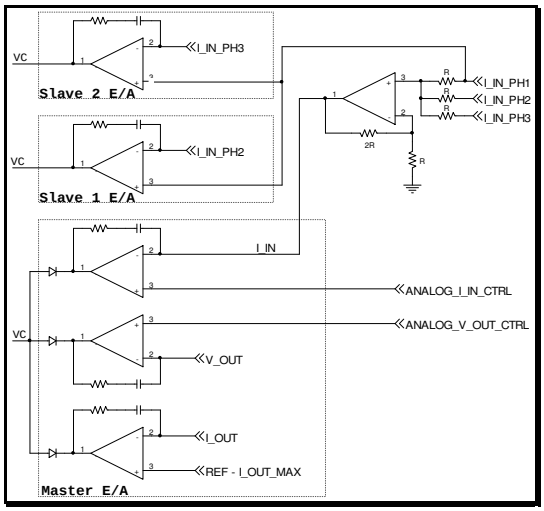

Fig. 44. Simplified error amplifier section

6.2 Analog control

The regulator requires two alternative methods of control – manual (local) control and ability to accept analog signals coming from fuel cell controller. This fairly simple circuit is shown in Figure 45.

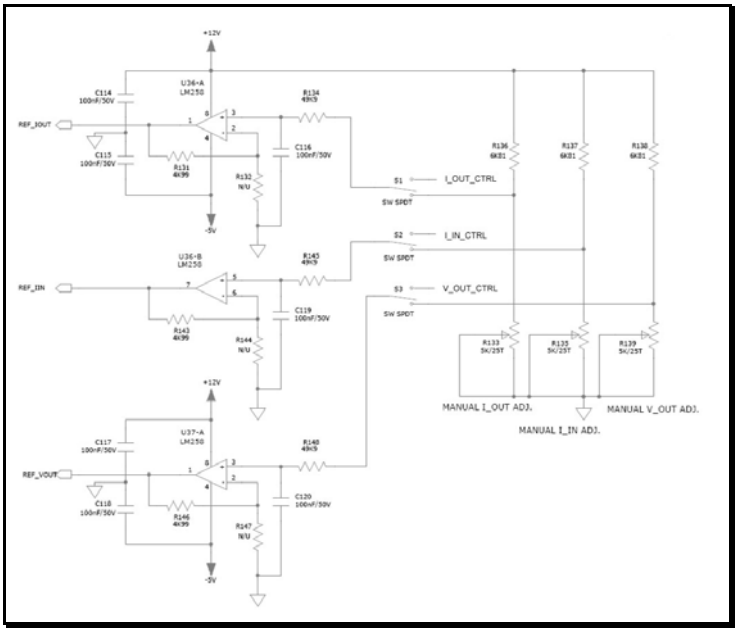

Fig. 45. Analog control section

Single-Pole-Dual-throw (SPDT) switches are used to select potentiometers for manual control or analog signals. Input and output current and output voltage are parameters that need to be regulated. In finished system only analog signals will be used in order to be able to dynamically change settings depending on the current state of the fuel cell system. In the future it is possible that this will evolve in a digital communication via serial interface.

6.3 Circuit protections

As indicated in Chapter 4.2, there are three major protections making sure that regulator always stays within the safe operating area:

- Output current limit
- Overvoltage protection
- Reverse current protection
- Overload protection
- Thermal protection

Output current limit circuit sets absolute maximum output current. When the limit is reached, the regulator will start reducing the output voltage in order to keep output current at the limit. The circuit is designed as a separate error amplifier with fixed reference voltage, as seen in the Figure 44 above. This limit is set at maximum specified output current, 150 A.

Overvoltage protection is derived as a simple comparator monitoring output voltage relative to the fixed reference voltage. The circuit schematic is shown in Figure 46.

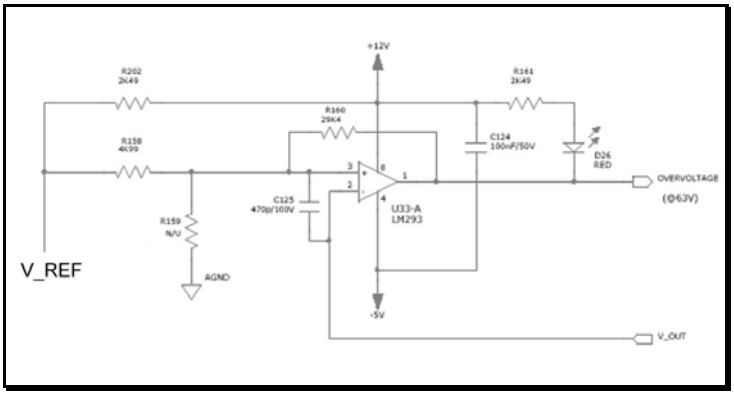

Fig. 46. Overvoltage protection circuit

The limit is set to 63V. If the output voltage exceeds the limit, unit will shut down and generate fault signal to inform the fuel cell regulator of an abnormal condition.

Reverse current protection is required to prevent current flowing into the fuel cell. This is potentially hazardous condition - the current flowing into the fuel cell will cause Hydrogen pressure and temperature to increase with possibility of damaging fuel cell membrane and overstressing Hydrogen tank. The protection is set to detect negative output current and to shut down the unit while simultaneously flagging the fuel cell controller of an error that requires an immediate attention.

Overload protection circuit reacts when the output current increases above the level of the output current limit (such as in short circuit situation). The goal is to shut down the

regulator, but also to send signal to the fuel cell controller to quickly turn off input power via the main system contactor. This is necessary as boost converter does not have inherent short circuit protection and overload will cause uncontrolled output current limited only by circuit parasitics.

If there is a short circuit at the output, current will flow through regulator's rectifier diodes, all 18 of them (6 per phase). Surge current rating for the chosen diode (STPS30SM100S) is 530A (non-repetitive for 10ms) and 18 diodes will have theoretical capacity of over 9500A. Even considering less than perfect current sharing, this is way above maximum current that the fuel cell can support in a short period of time, therefore contactor's reaction time of few milliseconds will be sufficiently fast to prevent damage to the regulator and fuel cell.

Finally, **thermal protection** ensures that the maximum circuit temperature never exceeds safe ratings. Temperature is measured by an NTC resistor (NTC signal) which is located on the IMS board hosting power semiconductors (MOSFET switches and Schottky rectifiers). Considering possibility of very heavy loads at elevated ambient temperature and tight packaging, it is likely that, at times, the regulator circuitry will operate at high temperature. In order to provide adequate warning that critical temperature is being approached, the thermal protection operates as follows:

- When unit's temperature reaches 75°C, which is the lowest threshold, a warning light will come on and maximum output current will be reduced by 25%. This helps reduce thermal load and slight loss of power gives operator warning without significantly affecting product's functionality.
- If temperature increases to 85°C a warning light comes on and power is reduced by 50% (TEMP_MED signal on the schematics). This more significant power loss indicates to the operator to change operating regime, perhaps to reschedule loads by moving on to lighter loads. The system still operates but functionality is somewhat limited.
- Further increase of temperature, to 95°C indicates approaching dangerous levels. Warning light is on and power drops to 25% (TEMP_MED_HIGH signal). At this point, the vehicle can still move easily but lifting power is severely limited. Operators are advised to allow sufficient time for unit to cool down.
- Finally, if the temperature reaches 100°C a shutdown signal is generated (TEMP_HIGH) and the regulator immediately stops. Thanks to thesystems storage battery, the vehicle can still move for a limited time, which is sufficient to complete the operation and relocate to a safe location.

Schematics of the thermal protection circuit is shown in Figure 47.

As the temperature of the unit starts going down, the regulator will be first enabled to work with 25% of power and then slowly the available power will increase to 50%, 75% and full power (100%), when temperature falls 3-5°C below the respective threshold.

7. Test results

The prototype unit was built to verify circuit and demonstrate regulator's operation. It was made in the form that resembles form factor of the final product. This will result in more accurate measurements than if a typical laboratory breadboard prototype was used. The prototype of the three phase boost fuel cell regulator is shown in Figure 48.

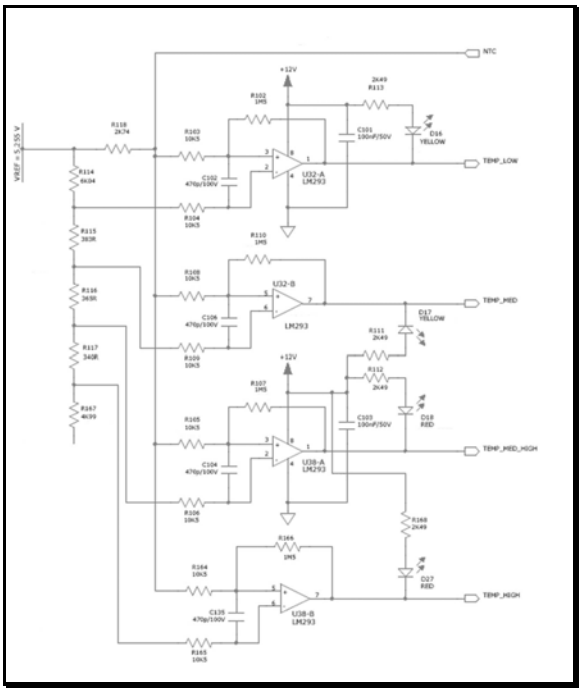

Fig. 47. Thermal protection circuit

Fig. 48. Photograph of the prototype unit

Base plate of the prototype is a heatsink hosting all the major parts of the regulator. Three input inductors occupy central location. Control board is located on the right side and underneath the board (not visible in the picture) is an IMS board with power semiconductors.

7.1 Measurements

The converter was tested over the full operating range. There were no significant problems found. Some improvements are possible and they will be considered for the future work. They will be described in more details later. Most importantly, testing confirmed that input inductors perform adequately, efficiency meets requirements and circuit waveforms are clean indicating low level of electromagnetic emissions.

For the waveforms captured below, the converter operated with the following nominal conditions (which are representative of the real operation in a fuel cell system):

- Input voltage: 28V
- Output voltage: 41V
- Input current: 149.8A
- Output current: 100A

In this mode of operation efficiency was calculated as 97.7% which is an excellent number, in compliance with the original specification requirement.

Input inductor current of each individual phase is shown in Figure 49.

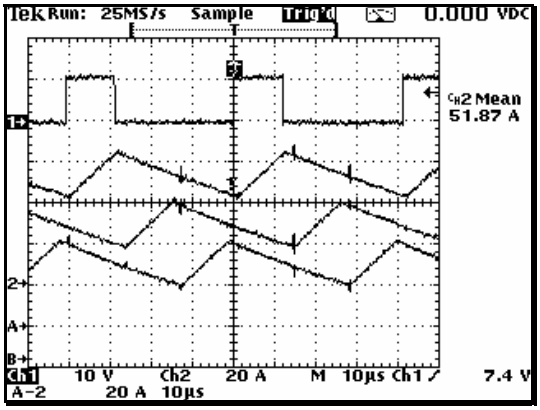

Fig. 49. Input inductor current waveforms of each individual phase

The upper waveform shows gate signal of the Phase 1 MOSFET, which is used as a timing reference. Input inductor current of Phase 2 and Phase 3 is shifted by 120° and 240°, respectively. Peak-to-peak value of the current is ~20A, (worst case ripple current of 24A).

Regulator's input current is sum of the three input inductor currents. The waveform is shown in Figure 50.

The effects of ripple attenuation are clearly visible: peak-to-peak input current ripple is less than 4A, compared to 20A for each individual phase. The waveform is very clean indicating stable operation.

The input current ripple being clean, low in amplitude and having 75kHz frequency is very benign and easy to deal with. A small capacitance at the input of the regulator will further reduce it without stressing the capacitors. Four capacitors, identical to those used in the output filter (470µF/63V) were added and input current ripple further reduced, to ~1App (Figure 51).

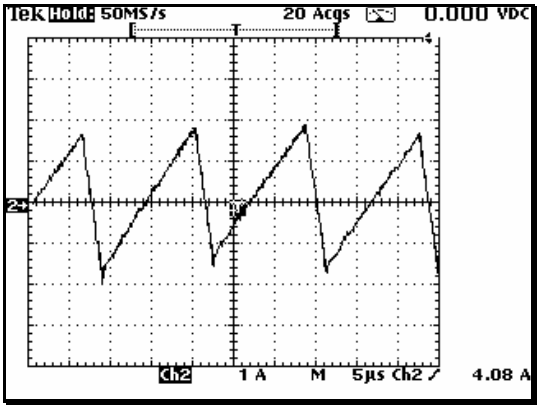

Fig. 50. Input current waveform

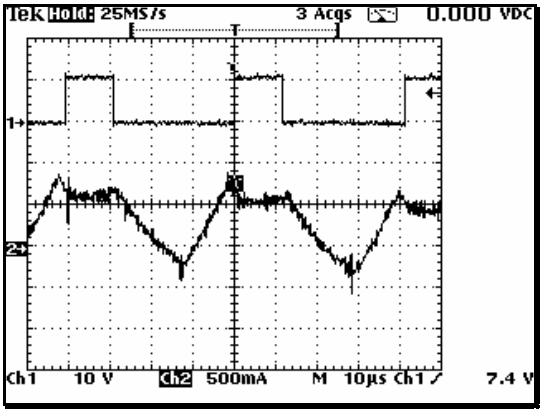

Fig. 51. Input current ripple with 4x470µF filter capacitance

Top waveform is again Phase 1 drive signal. By adding a small (for this power and current level) capacitance (1,880µF) across the input terminals, input ripple current is now reduced to 0.7% of the input current and is deemed perfectly acceptable for use with fuel cells which are normally very sensitive to the ripple content (typical spec for the ripple current is an RMS value of 1% or less).

Output current ripple was measured under the same operating conditions. Peak-to-peak value was approximately 0.5A, which is an excellent result. Waveform of the output current ripple is show in Figure 52.

This level of filtration is achieved with only 8460µF of output capacitance (18 capacitors of 470µF each). This is an excellent figure ensuring high quality battery charging and maintenance and no any negative effect on the load.

Finally, the conversion efficiency was calculated over the wide range of output power, and the plot is shown in Figure 53.

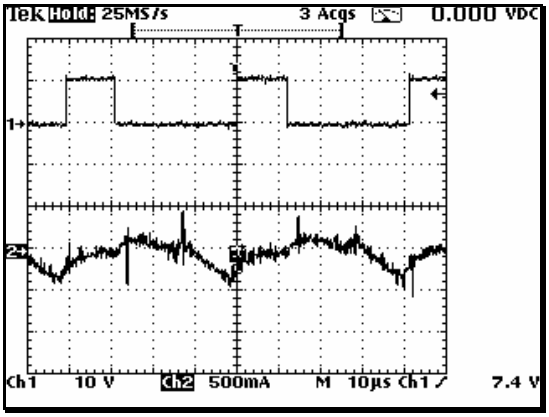

Fig. 52. Output current ripple

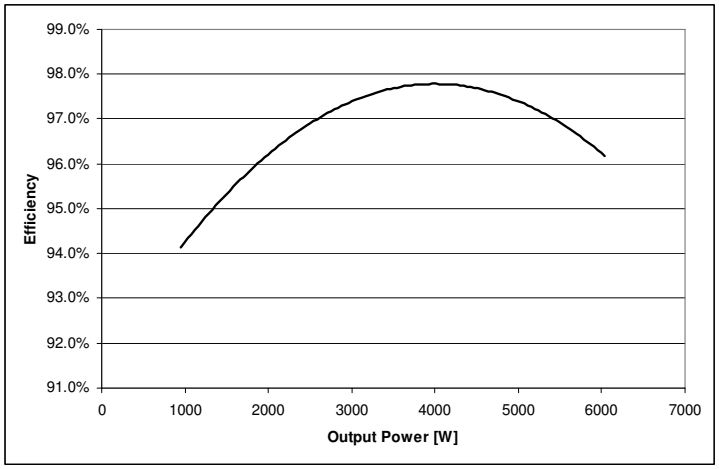

Fig. 53. Efficiency plot

Specification (Section 2.1) mandates efficiency of 94% minimum at 2kW output power and 96% above 2.5kW. As the efficiency plot illustrates, this requirement is met and exceeded by a reasonable margin.

8. Future work

During development and evaluation testing of the prototype, certain aspects were considered for possible improvement. Future work will address the following:

Synchronous rectification for increased efficiency. Replacing Schottky rectifier diodes with synchronously driven MOSFETS should, at least in theory, further reduce losses by substituting diode conduction loss ($V_F \cdot I_{out}$) for MOSFET conduction loss ($R_{ds(on)} \cdot I_{(RMS)}^2$). This requires more thorough analysis than simple component replacement, but the control circuit is designed to allow synchronous rectification, by providing complementary aoutputs.

Current sharing circuit also requires detailed analysis in order to ensure equal loading of all three phases during dynamic load changes. In order to perform the evaluation, a better understanding of the nature of the real life load is required. Relevant information is expected to be acquired during prototype testing in the field.

Circuit response to **fast current transients** will also need to be evaluated during field tests, once the typical values and operating regime is established.

Accuracy of **current measurement** is critical to ensure safe and reliable operation of the fuel cell, but also for regulator's operation. Measuring high DC current is quite a challenge, especially when the circuit needs to have very low cost. Proposed circuit based on a Hall effect sensors, but detailed evaluation over the wide load and temperature changes is required.

Microprocessor control shows promise of simplifying the circuit complexity by integrating supervisory functions of the regulator. Digital communication via serial interface will also be considered however, this aspect will be mainly driven by requirements and capabilities of the fuel cell controller, who is on the other end of the communication link.

Finally, **digital control loop** may also make sense in order to simplify the circuit and offer some unique benefits such as adaptive feedback and active current sharing. Development of a digital control loop is probably the most uncertain at the moment, considering state of the art and required multidisciplinary support.

9. Conclusions

The boost converter is one of the most commonly used power converter topologies covering wide range of input and output voltages, power levels and applications. Development of high performance and low cost semiconductors helped commercialize multiphase topologies offering multiple benefits at only a small price premium.

This paper addresses two of the most critical aspects of a multiphase boost converter: (1) input current ripple and (2) output capacitor RMS current. The basic equations for both parameters are derived in the first part of the paper. Building on this work a method for optimization of the number of phases is outlined in the second part.

By analyzing one practical application - a 5kW fuel cell regulator, interesting and somewhat surprising conclusion is reached: a three-phase converter operates with lower stress than an equivalent four-phase design. Simply increasing a number of phases does not always yield reduced component stress.

The fuel cell regulator has been thoroughly tested and some critical waveforms are shown in the last section as a practical illustration of the work done.

10. References

B. Fahimi, "*Automotive Fuell Cell Power Electronic Converters*", IEEE APEC Conference Seminar workbook, Vol. 3, February 2007.

B. Sasic, M. Zivanov, L. Nagy, M. Lazic, "*Power Regulator Design for Fuel CellApplications*", Electronics Journal, Vol. 11, No. 1-2, 2007, pp. 31-35.

B. Sasic, M. Zivanov, M. Lazic, "*Design of a Multiphase Boost Converter for HybridFuel Cell/Battery Power Sources*", Proc. of the XIV International Simposium on Power Electronics, Ee2007, December 2007, pp 1-5.

D. Liu and H. Li, "*A ZVS Bi-Directional DC-DC Converter for Multiple Energy StorageElements*", IEEE Transactions on Power Electronics, Vol. 21, No. 5, September 2006, pp.1513-1517

D. Liu at al., "*Design of a 6kW Multiple-Input Bi-Directional Dc-Dc Converter WithDecoupled Current Sharing for Hybrid Energy Storage Elements*", Proc. IEEE APECConference, February 2007, pp. 509-513.

J. Betten and R. Kollman, "*Interleaving DC/DC Converters Boost Efficiency and Voltage*", EDN Magazine, pp. 77-86, October 13, 2006.

J. Gavlik, "*Fuel Cell Basics*", Nuts and Volts magazine, May 2010, pp 47-55

J. L. Duarte, M. Hendrix and M. G. Simoes, "*Three-Port Bidirectional Converter for Hybrid Fuel Cell Systems*", IEEE Transactions on Power Electronics, Vol. 22, No. 2, March2007, pp. 480-487

J. Tsai *et al*., "*Interleaving Phase Shifters for Critical-Mode Boost PFC*", IEEE Transactions on Power Electronics, Vol. 23, No. 3, pp. 1348-1357, May 2008.

K. Jin, X. Ruan, " *Hybrid Full Bridge Three-Level LLC Resonant Converter – A Novel DC-DC Converter Suitable for Fuel-Cell Power System*", IEEE Transactions on Industrial Electronics, Vol. 53, No. 5, October 2006, pp. 1492-1503.

M. O'Loughlin, "*Advantages of Interleaved Boost Converters for PFC*", EDN Magazine,March 30, 2006, pp. 75-78.

M. Zhang, M. Jovanovic, F. Lee, "*Analysis and Evaluation of Interleaving Techniques in Forward Converters*", IEEE Transactions on Power Electronics, Vol. 13, No. 4, Luly 1998, pp. 690-698.

N. D. Benavides and P. L. Chapman, "*Mass-Optimal Design Methodology for DC-DCConverters in Low-Power Portable Fuel Cell Applications*", IEEE Transactions on PowerElectronics, Vol. 23, No. 3, May 2008, pp. 1545-1555

S. R. Moon at al., "*Multiphase Isolated Dc-Dc Converters for Low-Voltage High-PowerFuel Cell Applications*", Proc. IEEE APEC Conference, February 2007, pp. 101-1016.

T. Nussbaumer, M. Baumann, J. Kollar, "*Comprehensive Design of a Three-PhaseThree-Switch Buck-Type PWM Rectifier*", IEEE Transactions on Power Electronics, Vol. 22,No. 3, March 2007, pp. 551-562

X. Kong and A. M. Khambadkone, "*Analysis and Implementation of a High Efficiency,Interleaved Current-Fed Full Bridge Converter for Fuel Cell System*", IEEE Transactions on Power Electronics, Vol. 22, No. 2, March 2007, pp. 543-550

Y. Yang and M. Jovanovic, "*Interleaved PFC Boost Converter with Intrinsic Voltage-Doubler Characteristic*", Proc. IEEE Power Electronics Specialist Conference (PESC), 2006.

Z. Jiang and R. A. Dougal, "*A Compact Digitally Controlled Fuel Cell/Battery HybridPower Source*", IEEE Transactions on Industrial Electronics, Vol. 53, No. 4, August 2006, pp.1094-1104

Micrometals, "*200°C Series – High Temperature Powder Cores For PowerApplications*", Databook, 2007.

Paths to Sustainable Energy
Edited by Dr Artie Ng

ISBN 978-953-307-401-6
Hard cover, 664 pages
Publisher InTech
Published online 30, November, 2010
Published in print edition November, 2010

The world's reliance on existing sources of energy and their associated detrimental impacts on the environment- whether related to poor air or water quality or scarcity, impacts on sensitive ecosystems and forests and land use - have been well documented and articulated over the last three decades. What is needed by the world is a set of credible energy solutions that would lead us to a balance between economic growth and a sustainable environment. This book provides an open platform to establish and share knowledge developed by scholars, scientists and engineers from all over the world about various viable paths to a future of sustainable energy. It has collected a number of intellectually stimulating articles that address issues ranging from public policy formulation to technological innovations for enhancing the development of sustainable energy systems. It will appeal to stakeholders seeking guidance to pursue the paths to sustainable energy.

InTech Europe
University Campus STeP Ri
Slavka Krautzeka 83/A
51000 Rijeka, Croatia
Phone: +385 (51) 770 447
Fax: +385 (51) 686 166
www.intechopen.com

InTech China
Unit 405, Office Block, Hotel Equatorial Shanghai
No.65, Yan An Road (West), Shanghai, 200040, China
中国上海市延安西路65号上海国际贵都大饭店办公楼405单元
Phone: +86-21-62489820
Fax: +86-21-62489821